SEASONAL VARIATION AND BIOLOGICAL EFFECTS ON MUDFLAT ERODIBILITY IN THE MINAS BASIN, BAY OF FUNDY

by

Jessica Carrière-Garwood

Submitted in partial fulfillment of the requirements
for the degree of Master of Science

at

Dalhousie University
Halifax, Nova Scotia
November 2013

TABLE OF CONTENTS

LIST OF TABLES

LIST OF FIGURES

ABSTRACT

The goal of this study was to investigate the effects of intertidal mudflat biofilms on sediment erosion in the Minas Basin of the Bay of Fundy, Canada. From April through November 2012, sediment cores were collected biweekly and eroded using a Gust microcosm. Half of the cores were eroded without undergoing prior treatment, while the other half were treated with bleach prior to erosion to destroy biofilms. Size-specific sediment retention by biofilms was evaluated by comparing the disaggregated inorganic grain size (DIGS) distributions of sediment resuspended from untreated and treated cores, while seasonal variation in natural sediment erodibility was assessed by focusing on the mass eroded from untreated cores only. Results show that biofilms preferentially retained clays and very fine silts (< 10 μm), and that overall sediment erodibility decreased from spring to fall. Results also indicate that abundance of the infaunal amphipod *Corophium volutator* and rainfall increased sediment erodibility.

List of Abbreviations and Symbols Used

Abbreviation	Description
CME	Cumulative mass eroded
DIGS	Disaggregated inorganic grain size
EPS	Extrapolymeric substances
HPLC	High performance liquid chromatography
MERIS	MEdium Resolution Imaging Spectrometer
S_I	Sortability index
RPM	Rotations per minute
TME	Total mass eroded
TSM	Total suspended matter

Symbol	Description	Units
C_D	Drag coefficient	$-$
i	Size class	μm
M	Mobility	$-$
p	P-value	$-$
ρ	Density of seawater	kg m^{-3}
r^2	Coefficient of determination	$-$
τ	Shear stress	Pa
τ_b	Shear stress at seabed	Pa
u_{100}	Flow velocity one meter above seabed	m s^{-1}
V	Volume fraction	$\%$

ACKNOWLEDGEMENTS

First and foremost, I must acknowledge the support and inspiration offered by Dr. Paul Hill throughout my Honours and Master's degrees. Over the last four years, Paul has provided me not only with tremendous opportunities to foster my scientific career, but also with generally great advice for life. He has been the best supervisor I could have hoped for.

As members of my thesis committee, Dr. Markus Kienast, Dr. Hugh MacIntyre, and Tim Milligan have all had a crucial part in the completion of my degree. Beyond sharing their ideas, they have, in turn, helped me gain valuable ship work experience, supported me through puzzling issues with a standard lab procedure, and offered their time in the field.

The list of people who contributed to this work is long, but it is important for me to recognize every one of them. At Dalhousie University, Claire Normandeau offered pleasant conversations in the office and crucial support with the pigment analysis, Rachel Cox was instrumental in the field and contributed all *Corophium* data, while Trina Whitsitt provided access to the instruments and support for the carbohydrate measurement procedure. In the Particle Dynamics Lab at BIO, Brent Law ensured the success of this study by providing funding, space and instruments, while Vanessa Page, Emma Poirier and Karen Devitt offered their time, in turn, to help with the never-ending erosions and digestions. At SMU, I am grateful to Dr. Danika van Proosdij and Casey O'Laughlin for sharing their field expertise, making the lives of Paul, Rachel and me much easier during sampling.

The good friends I made throughout my degree must also be thanked for keeping my sanity. In alphabetical order: Laura deGelleke with whom I enjoyed great life and scientific discussions over wine, Mathieu Dever who kept me motivated to work by having a weekly hour contest where the *laziest* of us bought coffee for the other, Victoria Dickinson for being my academic cousin since first-year calculus, Anna Katavouta who was always available for a walk to Tim Hortons and a good chat, as well as the climbing community in Nova Scotia who made me discover a new passion.

Finally, I must thank the Oceanography Department at Dalhousie University in its entirety for having made me one of their own during my time here. Funding for this project was provided by NSERC and OERA.

CHAPTER 1

INTRODUCTION

1.1 Biofilms and fine sediment erosion

Coastal environments are rich in examples of the role flora can play in erosional processes. Rocks, for instance, experience chemical weathering from the acidic compounds released by lichens, as well as physical weathering by the root systems of plants that break them into smaller pieces. On river banks and ocean shores, however, root systems tend to prevent erosion by retaining soil and sediment. At the seafloor, a similar process takes place, although no root system is required. Instead, microalgae secrete substances that form mats, referred to as biofilms, that connect sediment grains, stabilize the sediment, and reduce erosion (*Holland et al.*, 1974).

Biofilms are an important component of coastal ecosystems as they provide substrate stability and serve as food for various benthic species, fish and even birds in some areas (e.g. *Elner et al.*, 2005). By increasing sediment stability, biofilms can enhance their growth, and thus the amount of food available to primary consumers, because they reduce the amount of shading caused by suspended particles in the water column, which allows for more photosynthesis in communities that are not otherwise nutrient-limited. The close association between biofilm growth and sediment erosion highlights the need for studies of biofilm-sediment interactions, in order to fully capture the ecological and sedimentary dynamics of coastal ecosystems. The work presented in this thesis aims to capture some of those interactions by focusing on the effects of biofilms on size-specific sediment retention and on seasonal mudflat erodibility.

Sediment dynamics and biological communities are sensitive to the grain size of the seabed, yet very little is known about size-specific sediment retention by biofilms. The

regular field measurements of mudflat erodibility obtained as part of this study are unique in their nature and frequency, which will not only help shed light on the seasonal effects of biofilms, but will also serve as input parameters for future modeling work of the area.

1.2 Objectives

In general terms, the goal of this study is to identify associations between eroded sediment and biofilm properties. More specifically, this research has four objectives:

1. Simulate natural erosion using a Gust microcosm, and compare the mass and grain size properties of the eroded sediment, using a Multisizer III Coulter Counter to obtain sediment grain sizes.

2. Identify which grain sizes, if any, are preferentially retained by biofilms during erosion of an intertidal mudflat.

3. Measure properties of the biofilm present on the natural sediment using established methods:

    - Measure sediment chlorophyll *a* using fluorometry;
    - Measure sediment carbohydrate concentrations using a phenol-sulphuric assay and spectrophotometry;
    - Characterize microbial assemblages by identifying photosynthetic pigments via high performance liquid chromatography (HPLC).

4. Discuss the seasonal trends observed in mudflat erodibility in the context of biological measurements and previous research, such as that of *Tao* (2013).

1.3 Thesis organization

To provide the reader with sufficient information regarding biofilms and sediment dynamics, within the context of this work, a more detailed introduction to the field of research is included in chapter 2. Chapter 3 offers a description of the study site, as well as of all the methods used as part of this research. Results are presented in chapter 4 and are discussed in chapter 5, focusing first on the size sorting effect of biofilms and its impact on surface

sediment, and second on the overall seasonal mudflat erodibility. Finally, a summary of the main results and their implications is found in chapter 6.

CHAPTER 2

BACKGROUND

Suspended sediment plays an important role in coastal ecosystems. For example, the concentration and grain size characterization of suspended sediment affect light penetration in the water column (*Baker and Lavelle*, 1984; *Boss et al.*, 2001; *Slade et al.*, 2011), which has obvious repercussions for photosynthetic organisms, as well as for visual predators and their prey (*Utne-Palm*, 2002). Slight changes in hydrodynamic conditions, and hence sediment transport, can also impact sensitive benthic communities, as increased sedimentation risks smothering organisms, while a reduction in silt content may decrease organic matter availability (e.g. *Thrush and Dayton*, 2002). The abundance of *Corophium volutator*, a keystone species in the Bay of Fundy, has been linked to the grain size of mudflats (*Trites et al.*, 2005). Changes to the sediment balance of these flats could, therefore, have repercussions on the semi-palmated sandpipers (*Calidris pusilla*) that rely on *Corophium* as their main food source during migration (*Shepherd*, 1995).

Due to its powerful tides, the Bay of Fundy has long been looked at for the development of tidal energy, and a thorough understanding of its sediment transport dynamics is required to evaluate the potential impact of flow disruption on local ecosystems (*Greenberg and Amos*, 1983). Using satellite imagery obtained from MEdium Resolution Imaging Spectrometer (MERIS), total suspended matter (TSM) has been shown to vary seasonally in the Minas Basin of the Bay of Fundy, with highest concentration in March and lowest concentration in late summer (*Tao*, 2013). A numerical model of sediment transport in the Minas Basin is able to reproduce this seasonal pattern by changing the erodibility of mud in shallow areas (*Tao*, 2013). A reasonable hypothetical mechanism for changing erosion rates seasonally is the growth and decay of sediment biofilms (*Holland et al.*, 1974;

Sutherland et al., 1998a).

Sediment biofilms are formed by microphytobenthic organisms such as cyanobacteria and diatoms, as well as by the extrapolymeric substances (EPS) they secrete. The stabilizing effect of biofilms on sediment has been established in a variety of settings (*Holland et al.*, 1974; *Grant et al.*, 1986; *Sutherland et al.*, 1998b; *Lundkvist et al.*, 2007), and shown to reduce suspended sediment concentrations by limiting erosion due to the sticky nature of EPS secretions that enhance adhesion between particles at the seafloor. A better understanding of the interactions between biofilms and sediment transport is crucial to assess and predict water quality, because contaminants, such as trace metals, adsorb preferentially to fine particles (*Milligan and Loring*, 1997) and bind to biofilms (*Sutherland*, 1990). Recently, both biofilms and suspended particles have been shown to increase contaminant retention by the seabed, notably with DDT (*Guo et al.*, 2012). Other studies, for their part, described an increased survival of pathogenic bacteria in the sediment when biofilms were present (*Decho*, 2000; *Piggot et al.*, 2012).

As outlined above, the most obvious mechanism by which biofilms can have a seasonal influence on satellite-derived TSM estimates is by reducing sediment erodibility. Another mechanism, however, consists of changing the size composition of the suspended sediment, which would affect the optical properties of the water column perceived via satellite. Previous studies (*Holland et al.*, 1974; *van de Koppel et al.*, 2001) have linked biofilms and particle size, where biofilms were associated with increased silt and clay content in the seabed. Part of this process is due to the EPS being redistributed in the water column and enhancing flocculation, which increases the settling velocities of silt particles, and thus their delivery to the seafloor (*Bender et al.*, 1994; *Decho*, 2000; *Stal*, 2010). The role of biofilm on size-specific sediment resuspension has, however, largely been ignored and studies focussing on this aspect are scarce.

Holland et al. (1974) reported a reduction in sediment erosion from sand-silt mixtures when certain diatom species were grown, which was not apparent with sand only, but the study focussed on the overall amount of sediment eroded. These results are consistent with field observations by *Faas et al.* (1993) who reported natural sand flats initially mistaken for mudflats due to a cohesive sediment behaviour associated with biofilms. In another experiment, 1-μm and 5-μm particles were released into a recirculating flume, and biofilms grown on sand were shown to preferentially retain the larger, silt-sized particles (*Arnon*

et al., 2010). It was suggested that biofilm pore sizes allowed the larger particles to deposit within the biofilm, but not to be as easily resuspended as the finer particles. Similar results have been observed with natural biofilms subjected to erosion in a Gust microcosm, where fine and medium silts were preferentially retained, as opposed to clays (*Garwood et al.*, 2013). All of these studies, however, focused on sandy environments, although biofilms are a conspicuous characteristic of muddy intertidal sediment.

The primary goal of this study is to fill this gap by investigating the effects of biofilms on size-specific sediment resuspension in an intertidal mudflat. More precisely, sediment cores were collected from an intertidal flat in the Bay of Fundy, and erosion was simulated using a Gust microcosm. Natural biofilms at the site (including both microorganisms and EPS) were quantified using chlorophyll *a* and bulk carbohydrate measurements. Following a similar procedure to *Garwood et al.* (2013), half of the cores were eroded without undergoing prior treatment, while the other half were treated with bleach to destroy biofilms. The grain size of the sediment resuspended from both sets of cores were then compared to evaluate biofilm effects. The secondary goal of this study is to assess seasonal differences in natural sediment erodibility. These measurements will be useful for assessing the viability of the hypothesis that seasonal changes in erodibility of mudflats produce the observed annual cycle of suspended sediment concentration in the Minas Basin of the Bay of Fundy (*Tao*, 2013).

CHAPTER 3

MATERIAL AND METHODS

3.1 Site and sample collection

From April through November 2012, samples were collected biweekly from a macrotidal flat in Kingsport, Nova Scotia (45.15° N, 64.37° W, figure 3.1). Intertidal flats in the area experience slightly asymmetric semi-diurnal tides, with a stronger flood than ebb, and an average tidal range 2of 11.5 m (*Faas et al.*, 1993). To avoid diurnal and tidal influence on biofilm properties caused by migration of microorganisms (*Smith and Underwood*, 1998), as well as changes in sediment erodibility caused by flat exposure (*Paterson et al.*, 1990), samples were always collected 5 hours after high tide. Field days were also selected such that sampling occurred at the same point in the spring-neap cycle and at the same time of day.

The site was divided in 24 quadrats (1 m $\times$ 1 m), each of which had one edge in contact with one of two sampling piers. The sampling piers allowed cores to be collected without disturbing the surrounding mud, and consisted of wooden planks resting on wooden piles (figure 3.2). The piles were driven into the mud at the onset of the sampling period and were left in place for the duration of the study, while the planks were laid down for sampling and removed immediately after. Every sampling day, one main quadrat was randomly selected for the collection of eight large (diameter = 10 cm) sediment cores, ensuring that previously sampled quadrats were not resampled. Core tubes were inserted 10 cm into the sediment, dug out, and sealed prior to being transported to the lab. Nearby sediment was used to refill the holes in order to minimize disturbance to flow over the flats. Piles were also oriented as to minimize flow disturbance, and samples were taken as far from the piles as possible. Three additional, randomly selected quadrats were also sampled using 10-ml

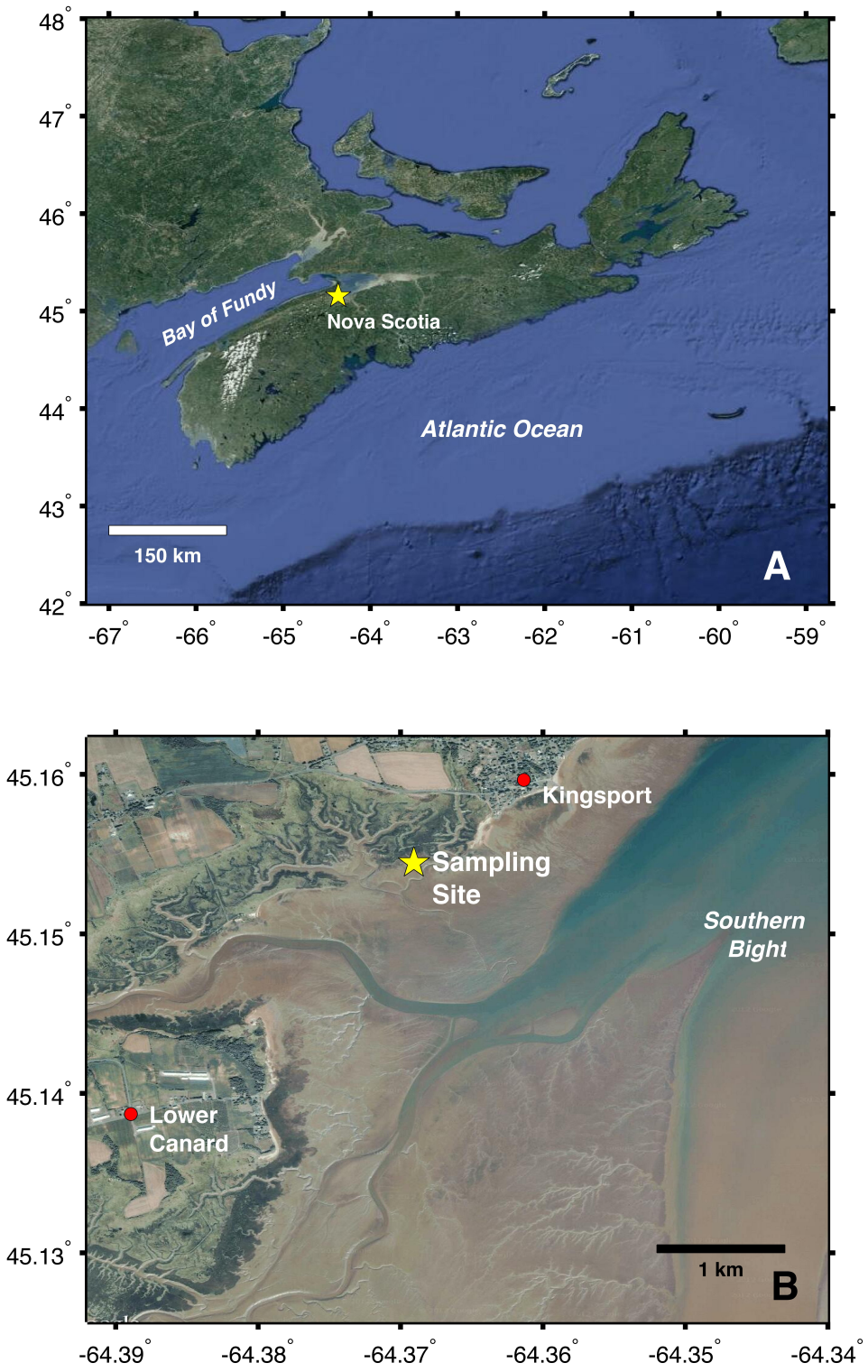

Figure 3.1: **A.** Yellow star shows sampling site location in relation to the Bay of Fundy and Nova Scotia (Canada). **B.** Map shows sampling site and immediate surroundings. *Map modified from Google Maps: Imagery ©2013 TerraMetrics (***A***), ©2013 Cnes/Spot Image, DigitalGlobe, Landsat (***B***), Map data ©2013 Google*

cut-off syringes to quantify site-scale variability in biofilm and sediment properties. Only the top 5 mm were kept and stored at $-80\,^{\circ}\mathrm{C}$.

3.2 Erosion and grain size analysis

Upon arrival to the lab, two of the eight large cores were subsampled using 10-ml cut-off syringes for biofilm and surface sediment measurements, and two were saved for macrofaunal counts. Only the top 5 mm were kept from the cut-off syringes and stored at -80°C until analysis. The remaining four large cores were then gently filled with seawater, taking care not to disturb the sediment surface. The refilling process was considered to have a minimal impact on the sediment surface, especially when compared to the tidal flooding of the flats. Following the procedure described in *Garwood et al.* (2013), two of the four cores were immediately eroded using a double-head Gust microcosm (*Tolhurst et al.*, 2000), while household bleach was added to the other two cores, in a concentration of 50 ml l^{-1}, to destroy the biofilm without interfering with the physical cohesion between sediment grains (*da S. Quaresma et al.*, 2004). The two treated cores were stored at $4\,^{\circ}\mathrm{C}$ overnight, in order for the bleach to have time to penetrate the sediment surface.

To simulate erosion, the Gust microcosm, which houses a rotating plate, was mounted on core tubes and controlled electronically to apply a uniform shear stress at the sediment surface for 20 minutes. Shear stresses ranging from 0.01-0.60 Pa were applied incrementally to each core. Throughout the erosion process, filtered seawater containing little to no sediment flowed into the Gust microcosm and flowed out of the system, carrying the resuspended sediment, as shown by a diagram of the Gust microcosm (figure 3.3). The seawater output was connected to a turbidity meter, allowing for continuous turbidity measurements. For each stress step, the outflowing seawater was collected and filtered to later obtain the mass and grain size distribution of eroded sediment. A sample of the inflowing filtered seawater was also collected for each erosion experiment in order to obtain background sediment concentrations, although minimal. The background sediment was then subtracted from the eroded mass. For each stress step, the cumulative mass eroded (CME) was calculated by summing the mass eroded at shear stresses weaker than or equal to the stress being considered. The total mass eroded (TME) from a core is equivalent to the CME at 0.60 Pa.

The disaggregated inorganic grain size (DIGS) distributions for each core and each stress

Figure 3.2: Picture of the field site, clearly showing the sampling piers.

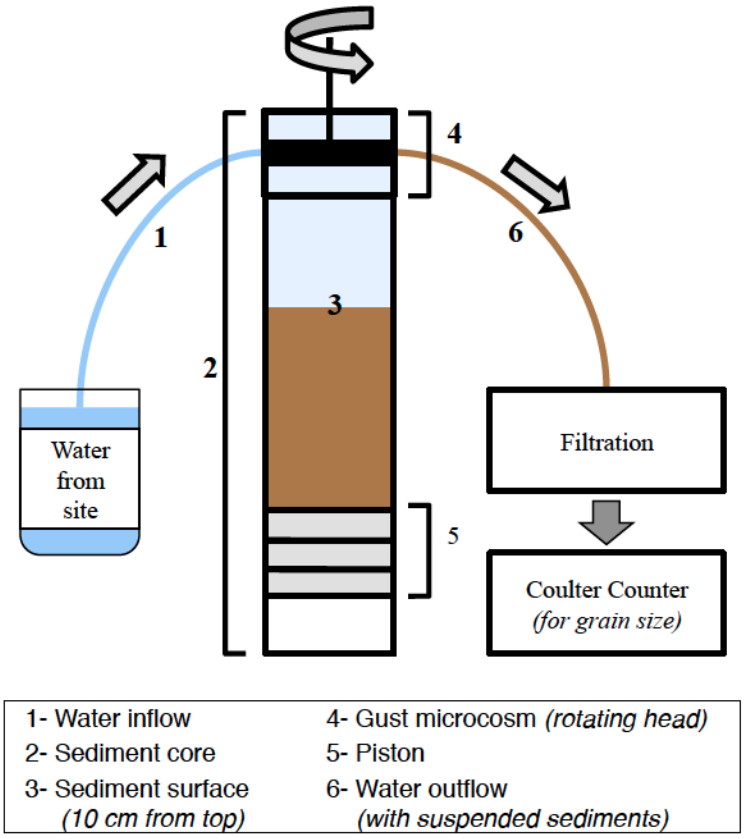

Figure 3.3: Diagram of the Gust microcosm, the device used to simulate erosion in the cores collected. The rotating head is connected to a computer controlling the rotation rate and water inflow, in order to produce shear stresses from 0.01-0.60 Pa.

step were then obtained using a Coulter Counter Multisizer III, following the procedure outlined in *Garwood et al.* (2013) and based on *Milligan and Kranck* (1991). In short, the filters containing the eroded sediment were first ashed using a low-temperature gas plasma asher and the remaining sediment digested using 30% hydrogen peroxide to remove any organic matter. The samples were then resuspended in a beaker of 1% NaCl electrolyte solution and disaggregated using an ultrasonic probe, immediately prior to obtaining grain size measurements with the Coulter Counter. In this study, tube aperture sizes of 30 and 200 μm were used. Data from each tube were merged using a custom-written Matlab code to produce size distributions of particles over the range of 1-100 μm (code available at *https://github.com/JessCG/MS3*). Surface sediment samples from three cut-off syringes collected from the main quadrat were also used to obtain surface DIGS distribution. The sampled depth reached 5 mm and the surface sample was homogenized before being digested with 30% hydrogen peroxide. These samples were assumed to be representative of the 1-mm active erosion depth previously reported by *Wiberg et al.* (1994). The surface samples were prepared for grain size analysis similarly to the filtered samples, but aperture sizes of 30, 200 and 400 μm were used, in case sediment grains > 100 μm were present. From the resuspended and surface DIGS, grain size mobility was calculated (*Law et al.*, 2008):

$$M_{i,\tau} = \frac{V_{i,\tau}\ resuspended}{V_i\ in\ original\ seabed}\ , \tag{3.1}$$

where M is mobility, i is a given size class, τ is the stress applied by the Gust microcosm, and V is the volume fraction of a size class in the total sediment sample. Mobility is thus an indication of how readily specific grain sizes are resuspended, compared to their abundance in the seabed. Mobility values below 1 indicate that the sediment grain size preferentially remains in the seabed during erosion, while mobility values above 1 indicate that the sediment grain size is preferentially resuspended from the seabed.

Mobility distributions as a function of grain size diameter (μm) were then described using a sortability index (S_I) (*Garwood et al.*, 2013). The index is a total sum of squares assigned a positive value if higher mobility values are found toward larger grain sizes, and a negative value if higher mobility values are found toward finer grain sizes. See Appendix C or *Garwood et al.* (2013) for all equations. This implies that the S_I value of a mobility distribution behaves similarly to a slope, but can also distinguish flatter distributions, or

those with peaks. Large positive S_I values are indicative of coarse sediment sorting, while large negative values are indicative of fine sediment sorting. S_I values close to zero show sediment grain sizes to be resuspended proportionally to their abundance in the seabed.

Finally, dry bulk sediment density was obtained by first drying and weighing the surface sediment from three cut-off syringes. The total dry weight obtained was then divided by the total volume collected (5 mm of sediment from syringes with diameter = 13 mm).

3.3 Biological measurements

3.3.1 Pigments

Chlorophyll *a* measurements were used as a proxy for photosynthetic biomass, despite the possibility that seasonal variation in irradiance would lead to variation in the carbon-to-chlorophyll ratio (*Langdon*, 1988). Measurements were obtained using triplicate surface samples collected with the cut-off syringes. The top 5 mm were kept and stored at $-80°$C. Before analysis, samples were thawed and 10 ml of 90% acetone was added as soon as the samples were no longer frozen. Samples were agitated in a cold sonifying bath and kept at $-20°$C overnight before being centrifuged at 4000 RPM for 7 minutes. The supernatant was analyzed using a Turner Designs fluorometer calibrated with pure chlorophyll *a* (Sigma-Aldrich) and equipped with Corning excitation filter 5-60 and emission filter 2-64 (*Goericke and Repeta*, 1993).

The concentration of additional photosynthetic pigments was measured using an Agilent 1100 high performance liquid chromatography (HPLC) system, equipped with a Zorbax Eclipse XDBC_{18} 150 mm $\times$ 4.6 mm HPLC column with a 5 mm particle size (Agilent Technologies), following a procedure based on *Wright et al.* (1991). Triplicate surface samples collected with the cut-off syringes were thawed at $4°$C overnight and 3 ml of 100 $\%$ acetone was added in the morning of analysis. Samples were vortexed and stored at $-20°$C for 1.5 hours to allow for the extraction to proceed. Thirty minutes into the extraction, samples were taken out of the freezer individually and sonicated with a probe set to pulse mode for 18 s before being returned to the freezer. The timing was determined by conducting tests to ensure the samples remained cool. Samples were then centrifuged at 4000 RPM for 7 minutes and the supernatant analyzed. For additional information regarding the HPLC protocol, see *DalU Method* in *Hooker et al.* (2012).

3.3.2 Carbohydrate content

The bulk carbohydrate content of the sediment (including microorganisms and EPS) was measured by conducting a colorimetric phenol-sulphuric assay as outlined in *Sun et al.* (1984), and modified from *Dubois et al.* (1956). Triplicate surface samples collected with the cut-off syringes were freeze-dried and 10-15 mg of dry sediment was transferred into glass test tubes for analysis. The precise weight was recorded. In turn, 800 μl of deionized water, 1 ml of 5% phenol (w/v), and 4 ml of 96% sulphuric acid were added to the sediment samples. The samples were thoroughly vortexed after the addition of phenol, as well as before and after the addition of sulphuric acid. The samples were then put in a water bath at 95°C for a total of 1 hour, with thorough vortexing after 30 minutes. After being allowed to cool to room temperature, the samples were centrifuged at 6000 RPM for 5 minutes, and analyzed using a Cary 4000 UV-Vis spectrophotometer from Agilent Technologies. Peak absorbance between wavelengths of 480-490 μm was recorded for each sample. D-(+)-Glucose (Sigma-Aldrich) was used to generate a standard curve with sample glucose mass ranging from 0-160 μg.

3.3.3 Macrofauna

Following a procedure similar to *Hicklin et al.* (1980), the macrofauna at the site was monitored by counting the number of *Corophium volutator*, polychaetes, amphipods, nematodes, bivalves and gastropods in two large cores (diameter and thickness = 10 cm) collected from the main quadrat. The sediment in the cores was screened with a 0.5 mm mesh and organisms soaked for 15 minutes in a solution of magnesium chloride (concentration of 75 g l^{-1}). The organisms were then stained with rose bengal and fixed in 10% formaldehyde for a few days before being transferred and stored in 70% ethanol. This work was carried out by Honours student Rachel Cox.

CHAPTER 4

RESULTS

4.1 Erodibility

4.1.1 Sediment behaviour without biofilm effects (treated cores)

The cumulative mass eroded (CME) of treated cores were similar throughout the 8-month study period (April to November 2012, figure 4.1, $CV_{0.60Pa}$ = 23%). When an Aquadopp was deployed at the field site, velocities above 50 cm s^{-1} were regularly measured one meter above the seabed (O'Laughlin, *personal communications*). Using $\tau_b = \rho\, C_D\, {u_{100}}^2$, where τ_b is the shear stress at the seabed (Pa), ρ is the density of seawater (1025 kg m^{-3}), C_D is the drag coefficient (a conservative low estimate of 2.5×10^{-3} was used, (*Wu et al.*, 2011)), and u_{100} is the flow velocity one meter above the seabed (m s^{-1}), it can be calculated that the site regularly experienced shear stresses above 0.6 Pa, consistent with bottom shear stresses presented in *Wu et al.* (2011) for the area. Further analyses of flat erodibility will, therefore, focus on the CME at 0.6 Pa, referred to as the total mass eroded (TME).

A Shapiro-Wilk test and a Grubbs' test for outliers were conducted to evaluate if the observed TME for treated cores could be considered a single, normally distributed population. It was found that the observed TME for treated cores did not deviate from a normal distribution (*Shapiro-Wilk,* $p = 0.8$), and did not contain significant outliers (*Grubb's,* $p = 0.3$). These results indicate that the variation observed in the sediment erodibility of treated cores was not statistically different from the variation observed in a normal distribution. Moreover, the hypothesis that the TME values were randomly distributed over time was not rejected when performing a non-parametric runs test using Matlab ($p = 0.24$), implying that no clear temporal trend could be identified in treated

sediment. In the runs test routine, the mean of the distribution is subtracted from each observation and the resulting sequence of negative and positive values is compared to what can be expected from a random sequence of negative and positive values. Only the signs of the resulting values are considered.

Overall, the normally-distributed variation observed in mass eroded from treated cores, as well as the lack of identifiable temporal trend in these data (figure 4.2), show that the sediment's susceptibility to experimental erosion did not vary significantly, nor systematically, throughout the study period. Trends observed in the untreated sediment will, therefore, be viewed as the result of biological factors only, as any trend dictated by the physical properties of the sediment would have been apparent in treated cores. The remainder of this thesis will focus on the untreated sediment behaviour and use the treated sediment data as controls.

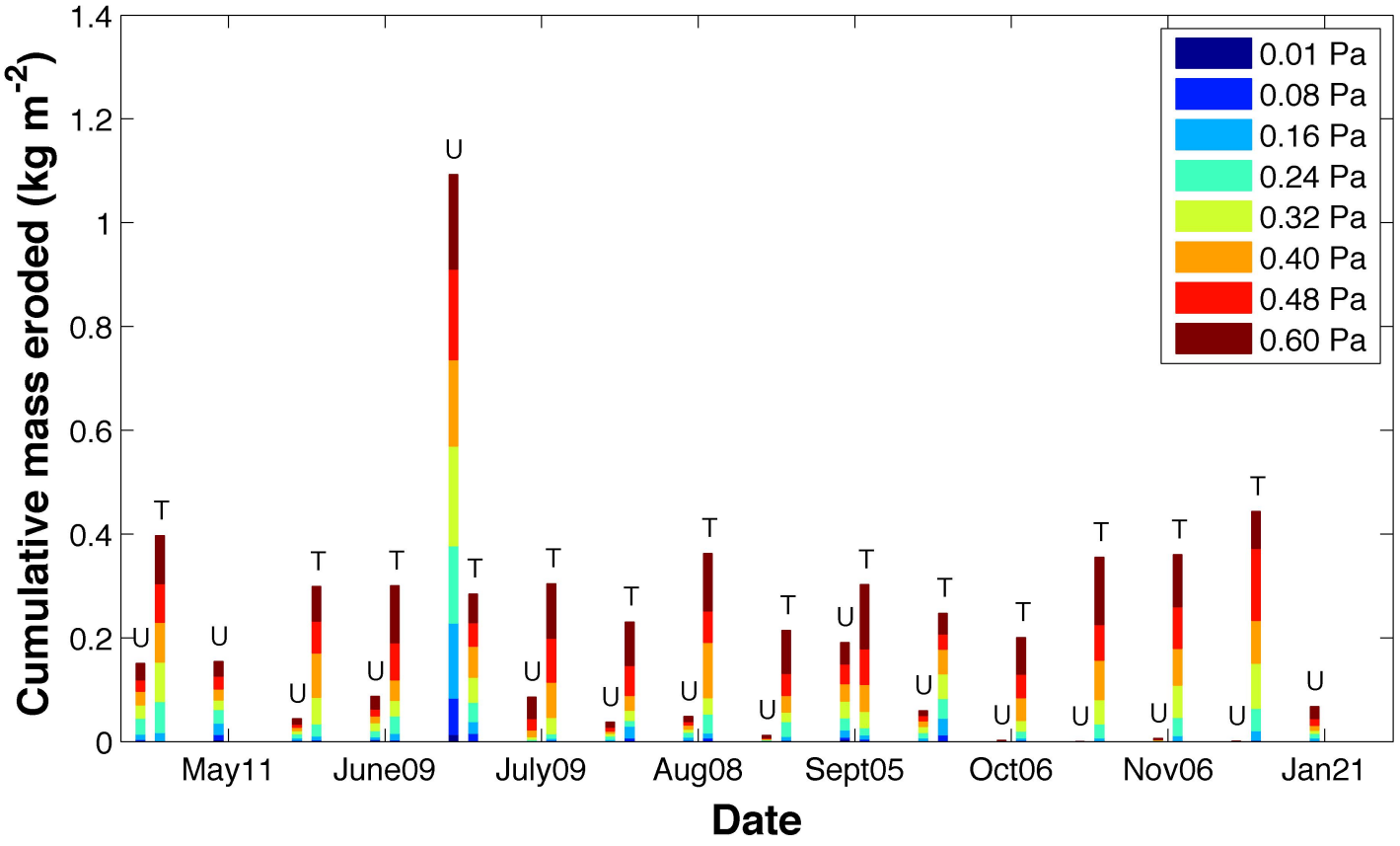

Figure 4.1: Cumulative mass eroded (kg m^{-2}) of untreated (U) and treated (T) cores for each collection date. When replicate cores were available, the trend displayed is an average of the duplicates.

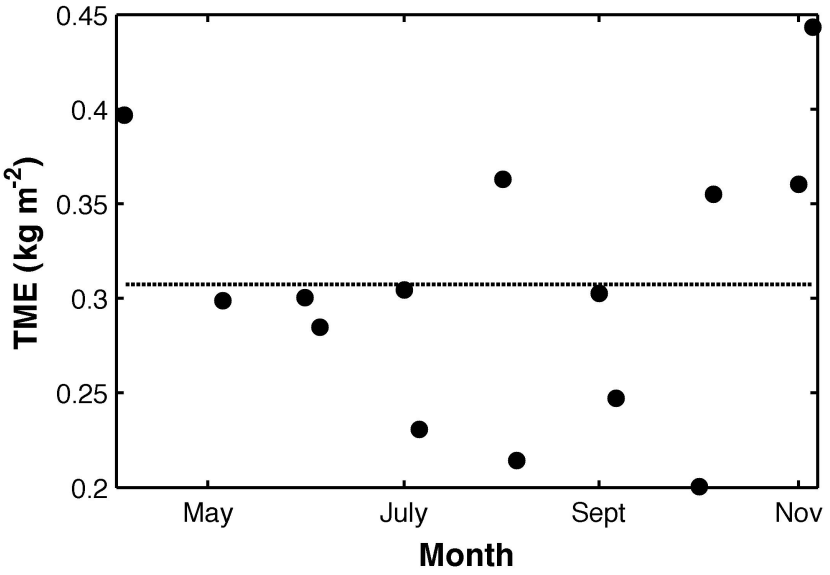

Figure 4.2: TME (kg m^{-2}) eroded from treated cores as a function of collection date. The dashed line shows the mean of the distribution, used to perform a non-parametric runs test.

4.1.2 Natural sediment behaviour, including biofilm effects (untreated cores)

The total mass eroded from untreated cores generally decreased from spring to fall, with two notable increases in TME in June and September (figure 4.3). The high mass eroded on June 24 was almost a full order of magnitude higher than any other untreated cores, while the mass eroded on September 5 was higher than other cores collected at that time of year. Plotting TME and *Corophium* abundance, as well as TME and rain, as a function of sampling date (figure 4.4), shows that the TME peaks on June 24 and September 5 coincided with the highest *Corophium* and rain values of the entire field season, two factors known to increase sediment erosion (*Daborn et al.*, 1993; *Paterson et al.*, 1990, 2000; *Tolhurst et al.*, 2008b).

In order to remove the effects on TME assumed to be associated with *Corophium* and rainfall, and focus on seasonal scale variability, a linear regression excluding data from June 24 and September 5 was carried out. A square root transformation of the TME data was first carried out because the decrease in TME showed some curvature, although the overall fit did not vary much ($r^2 = 0.67$ and $r^2 = 0.72$ for original and transformed data respectively, with $p = 0.0002$ for both). A statistically significant trend indicates

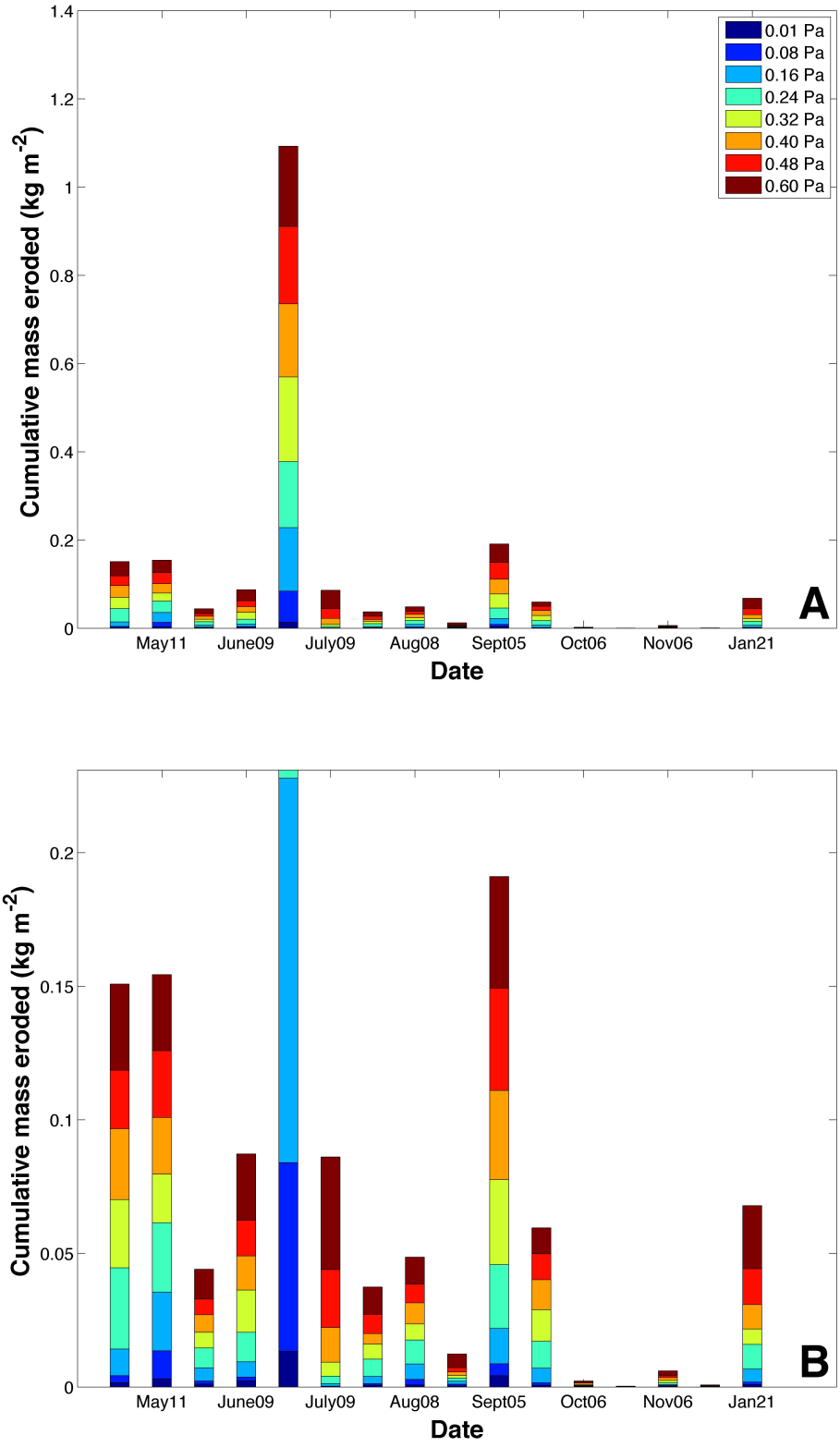

Figure 4.3: **A.** Cumulative mass eroded (kg m^{-2}) for all untreated cores. **B.** Scale of y-axis adjusted to focus on cores dwarfed by the June 24 data.

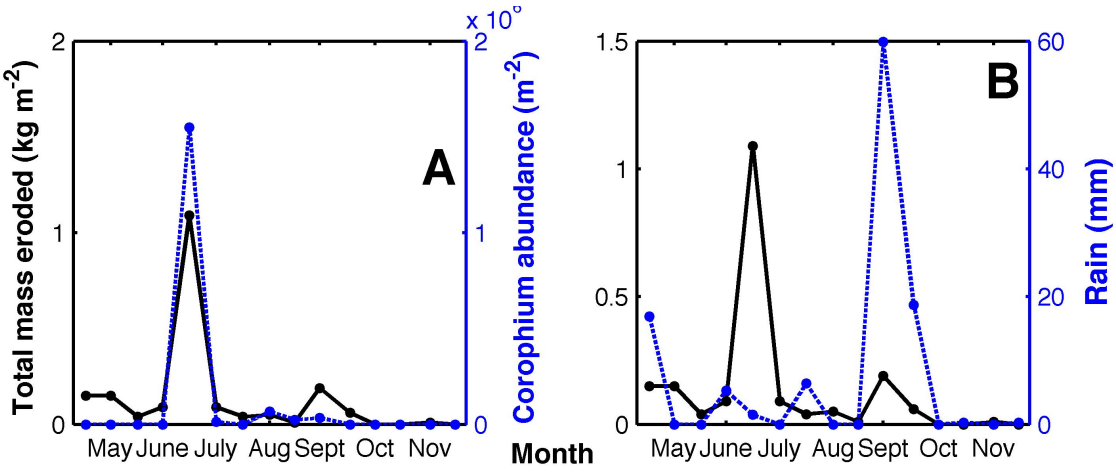

Figure 4.4: **A.** Total mass eroded (kg m^{-2}) and *Corophium* abundance (m^{-2}) for all sampling dates. **B.** Total mass eroded (kg m^{-2}) and rain on sampling day (mm) for all sampling dates.

that mudflat erodibility decreased drastically from April through November 2012, from a maximum of 0.15 kg m^{-2} to a minimum of 0.0003 kg m^{-2} (figure 4.5).

4.2 DIGS

4.2.1 Surface

An average surface disaggregated inorganic grain size (DIGS) distribution was generated for each month of field work, using triplicate surface samples collected every field day. Surface sediments were finer in May and June than they were in July, August, and September 2012 (figure 4.6). The month of October had the coarsest sediment grain size distribution, while in November, surface sediment became finer, returning to textures similar to those observed in May and June. Based on the Folk classification (*Folk*, 1954), the flat can be classified as mud for the duration of the sampling season, except for October, where seabed texture reaches the lower limit of sandy mud (table 4.1).

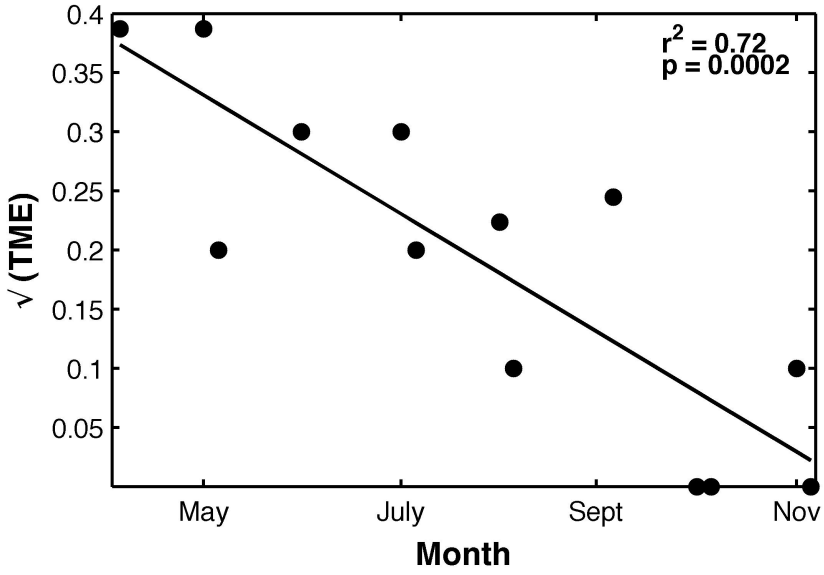

Figure 4.5: Square-root transformed TME (kg m^{-2}) values as a function of month. Data for June 24 and September 5 were removed. A statistically significant linear trend ($r^2 = 0.72$, $p = 0.0002$) is also shown.

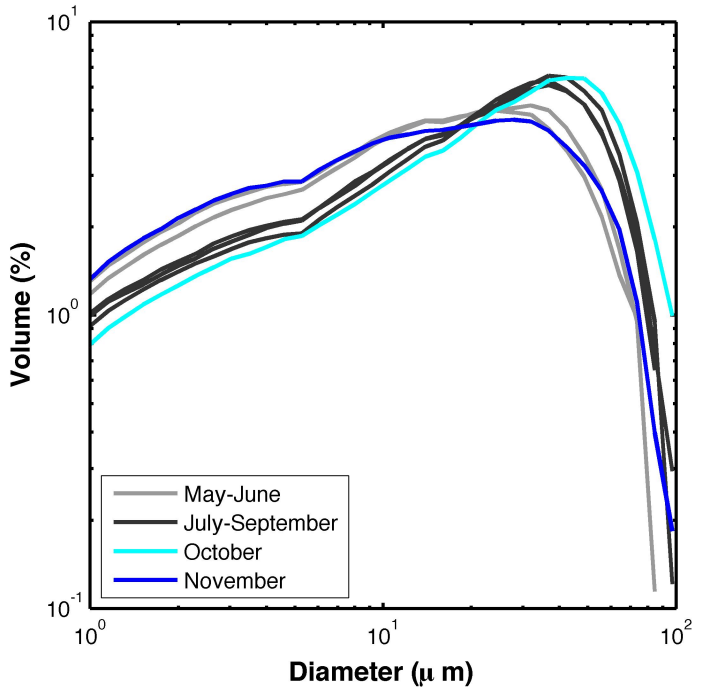

Figure 4.6: Surface DIGS as a function of diameter (μm). Each monthly average was calculated from triplicate samples collected every field day.

Table 4.1: Grain size characterization of surface sediment. Consecutive months with similar surface DIGS were grouped, as identified in figure 4.6.

Months	$\% \leq 4\mu m$	$\% \, 4-10\mu m$	$\% \, 10-63\mu m$	$\% \geq 63\mu m$
May - June	21.6	19.1	56.7	2.5
July - Sept.	16.2	14.5	63.4	5.9
October	13.9	12.9	62.7	10.4
November	23.3	19.7	53.3	3.6

4.3 Mobilities

4.3.1 Treated vs. untreated cores

Mobility distributions were obtained for each stress step and each core by dividing the volume fraction in a size class of the resuspended sediment by the volume fraction of that size class in the surface sediment (equation 3.1). Average mobility distributions, as a function of diameter (μm), were obtained for both treated and untreated core duplicates. Sample data are shown for cores collected on June 9, 2012 (figure 4.7), but all data can be found in appendix A. At shear stresses < 0.24 Pa, fine sediment was proportionally more mobile in treated cores than in untreated cores.

In order to investigate the statistical significance of this observation, the sortability index (S_I) of each average mobility distribution was obtained. Recall that S_I can be thought of as a slope, where large positive/negative values indicate preferential resuspension of coarse/fine sediment. The S_I values of untreated cores were then subtracted from that of their corresponding treated cores. A positive value in the differential sortability, S_I (treated - untreated), thus indicates that coarser grains were resuspended from the treated core than from the untreated core, while a negative value indicate that finer grains were resuspended from the treated core. A value close to zero indicates that similar grain sizes were resuspended in both treated and untreated cores.

Differential sortabilities at 0.08 and 0.16 Pa were statistically different from zero (*Wilcoxon signed-rank test*, $p = 0.004$ and $p = 0.008$, respectively, figure 4.8). In both cases, S_I was overall negative, indicating that a greater proportion of fine sediment grains was resuspended in treated cores. For this analysis, data from the months of October

and November were excluded because the limited resuspension exhibited by untreated cores did not yield sufficient sediment samples for reliable grain size distributions to be obtained.

In order to identify more precisely the grain sizes preferentially eroded in treated cores, the grain sizes where mobilities in treated cores exceeded mobilities in the corresponding untreated cores were isolated (shaded area in figure 4.9), focussing on shear stresses of 0.08 and 0.16 Pa only. Figure 4.9 shows that grains preferentially resuspended in treated cores at 0.08 Pa covered a range of 1.00 - 6.06 μm, while they covered a range of 1.00 - 9.19 μm at 0.16 Pa. The sediment grains preferentially resuspended from treated cores at 0.08 and 0.16 Pa were also calculated to be, on average, 2.35 and 3.31 μm respectively. These two values were found to be statistically distinct (*Wilcoxon signed-rank test*, $p = 0.02$).

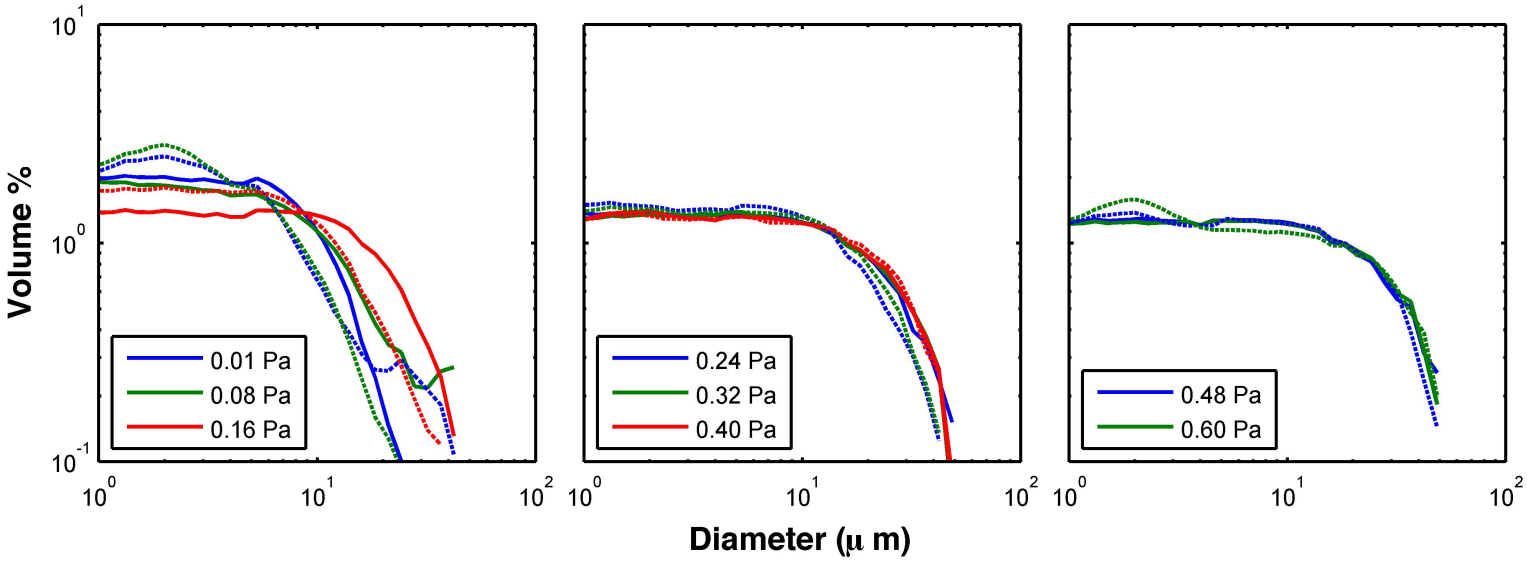

Figure 4.7: Mobility as a function of diameter (μm) for cores collected on June 9, 2012. The solid lines show the average mobility of duplicate untreated cores, while the dotted lines show the average mobility of duplicate treated cores.

4.4 Biological measurements

After an initial peak on June 9, the bulk carbohydrate content of the sediment (mg of carbohydrate g^{-1} of sediment) decreased throughout the summer, followed by an increase in the fall (figure 4.10). A similar trend was observed in the chlorophyll *a* levels at the sediment surface (mg of chlorophyll *a* m^{-2}), although no peak was observed prior to chlorophyll decline, and some increase was observed in August (figure 4.11). *Sutherland et al.* (1998b) reported erosion rates to be negatively related to bulk carbohydrate content, as well as chlorophyll *a* concentrations, with the strongest negative correlation obtained when considering the bulk carbohydrate to chlorophyll *a* ratio. In this study, none of these measurements were found to be correlated with TME. When compared with other properties of the sediment, bulk carbohydrate consistently led to higher correlations than chlorophyll *a* or carbohydrate-to-chlorophyll ratio, and was thus selected as the preferred biofilm proxy for further analysis.

The trend observed in bulk carbohydrate was found to be strongly correlated with the fine fraction ($\% \leq 10\ \mu$m) of surface sediment ($r^2 = 0.78$), as well as dry bulk density (kg m^{-3}) ($r^2 = 0.76$, figure 4.12), but not with sediment erodibility. The fine fraction of surface sediment was also strongly correlated with dry bulk density ($r^2 = 0.66$, figure 4.12), as would be expected due to the higher porosity of fine sediment than of coarse sediment. Results from the HPLC analysis indicated that the biofilm was dominated by diatoms throughout the 8-month study period. More specifically, fucoxanthin was identified in all samples, but no other marker pigments.

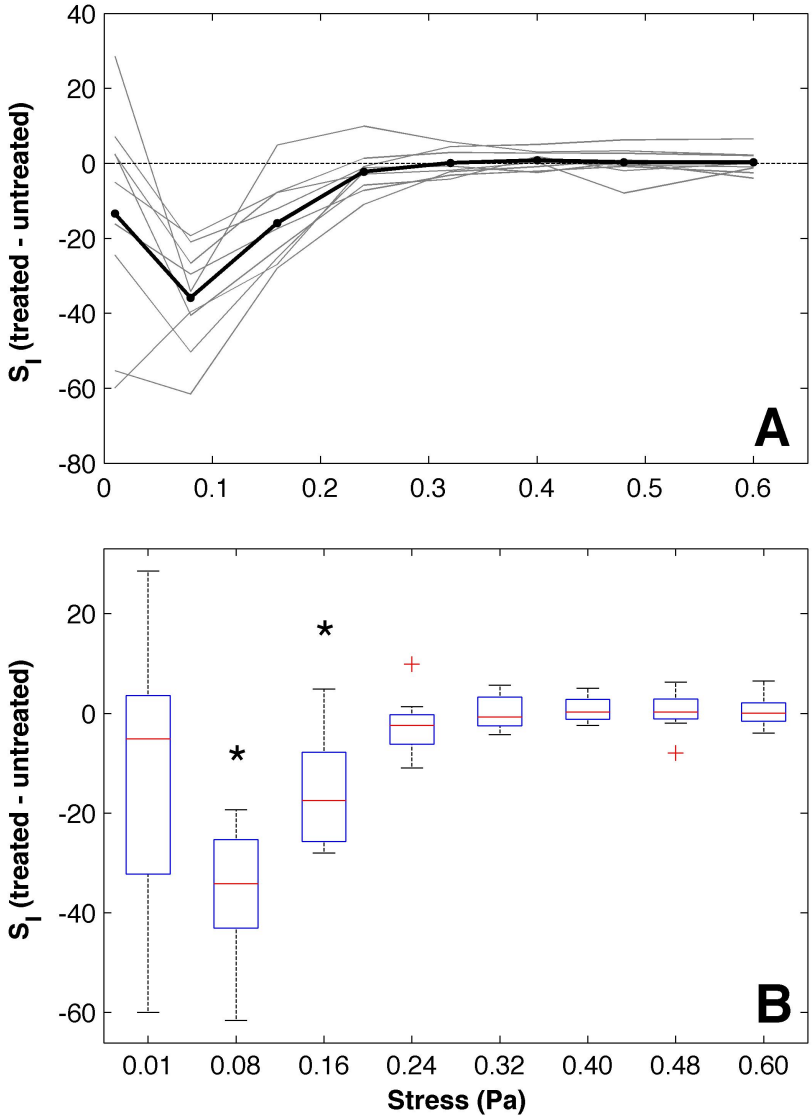

Figure 4.8: **A.** Differential sortability (S_I) of treated cores, when compared to untreated cores, as a function of stress (Pa). Grey lines represent S_I values from May to September 2012. **B.** Boxplot representation of the differential sortabilities in **A**. Stresses for which the mean sortability of treated cores are statistically lower than that of untreated cores are shown by an *asterix*.

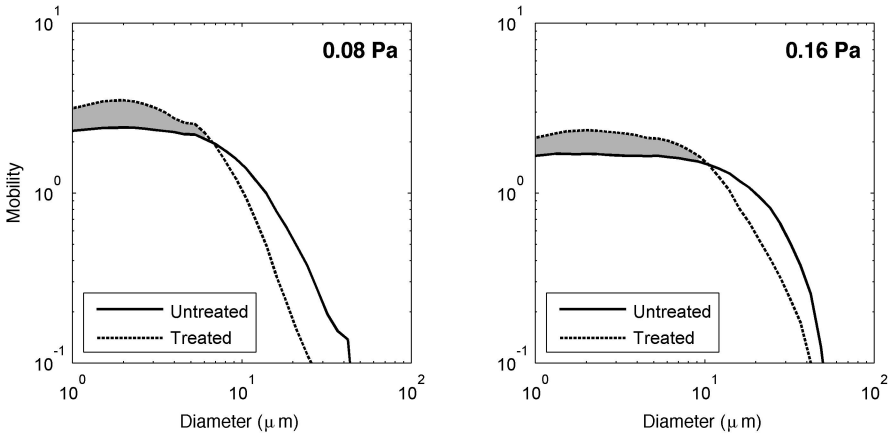

Figure 4.9: Average mobility from May to September 2012, as a function of grain diameter (μm) for shear stresses of 0.08 and 0.16 Pa. The shaded area represents the grain sizes preferentially resuspended when biofilms were destroyed.

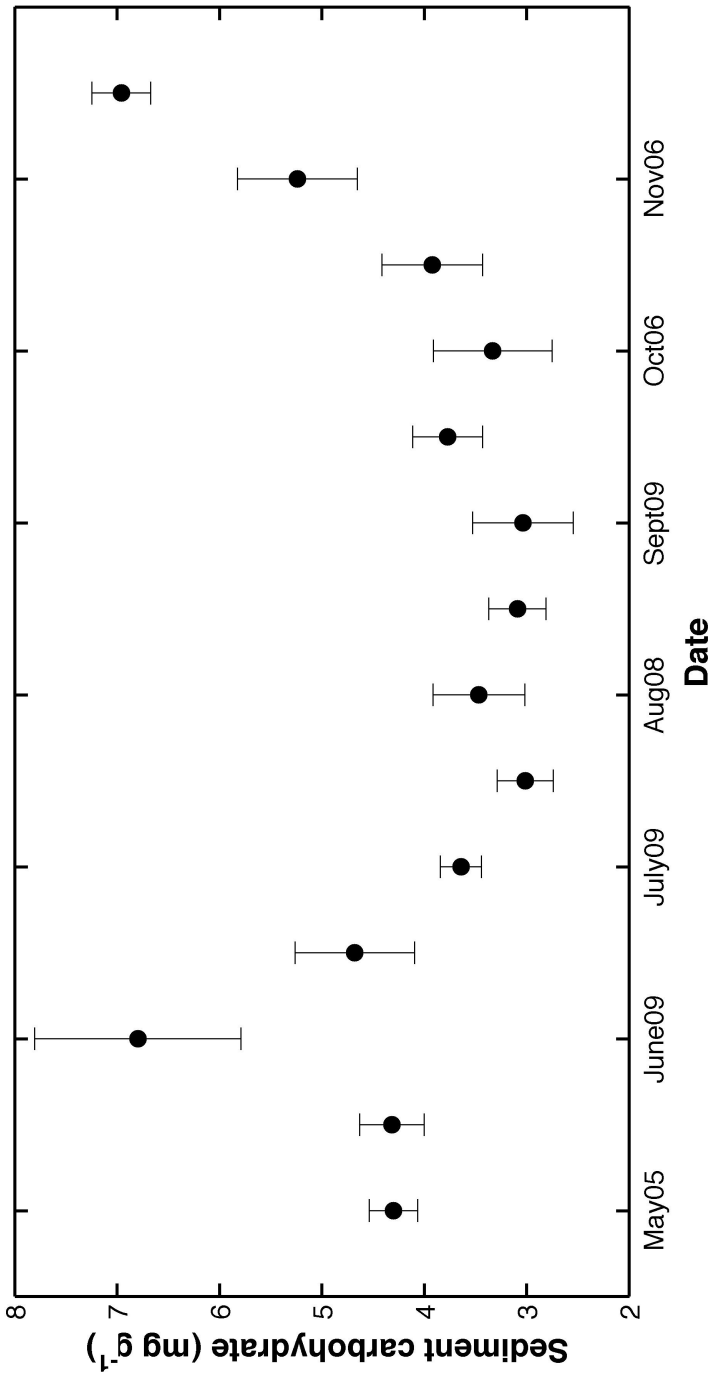

Figure 4.10: Bulk carbohydrate concentration in sediment (mg g^{-1}) from May to November 2012. Each colour represents triplicates from a single cut-off syringe. For each field day, three syringes were collected for carbohydrate analysis.

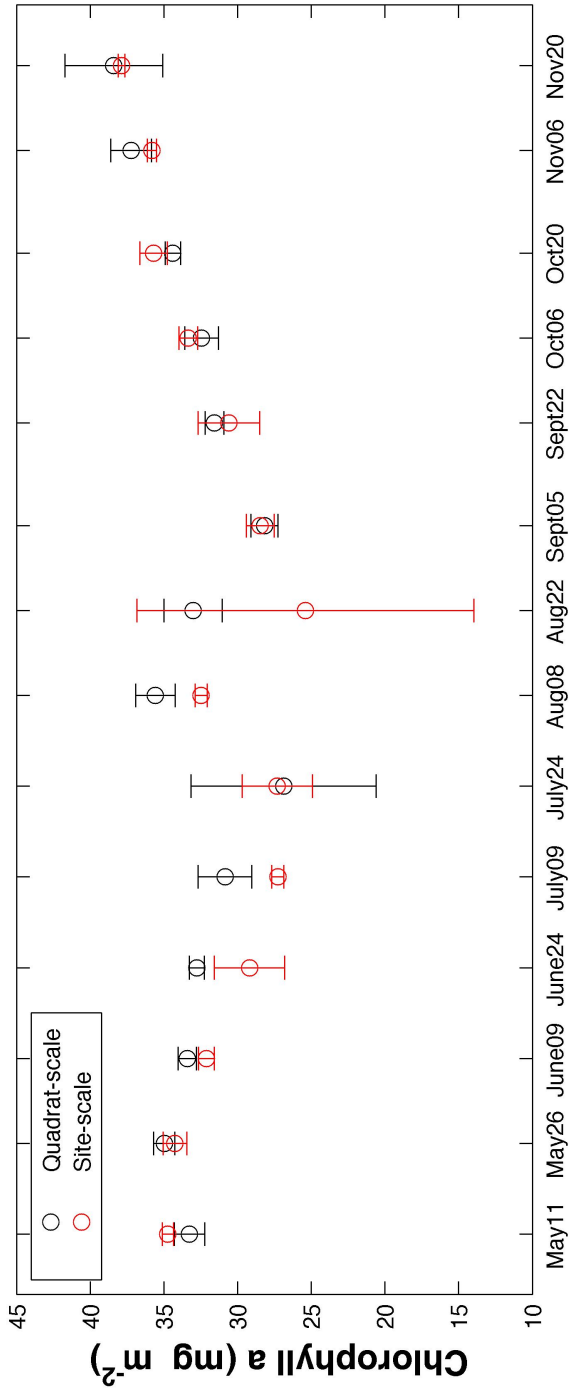

Figure 4.11: Chlorophyll *a* concentration in sediment (mg m^{-2}) from May to November 2012.

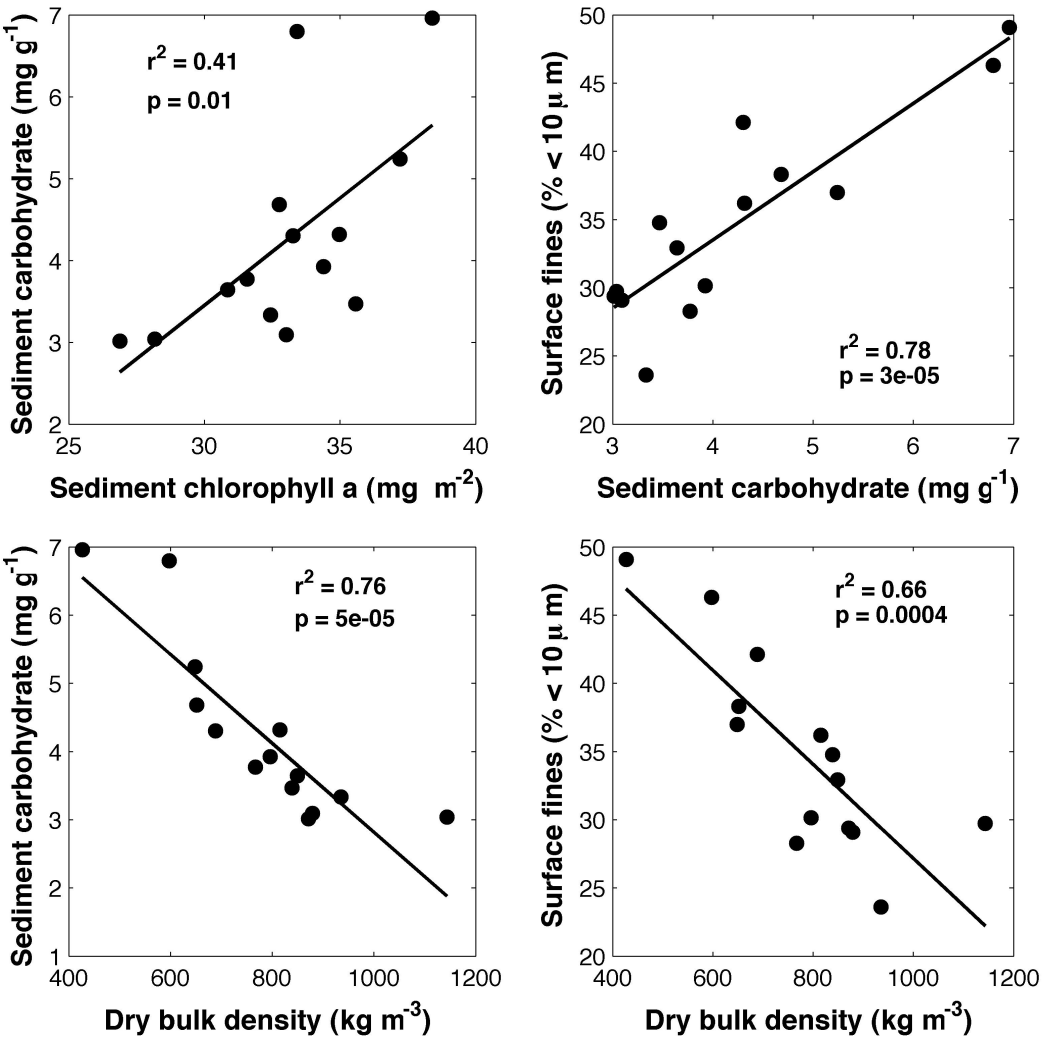

Figure 4.12: Statistically significant relationships between selected biological and physical properties of the sediment: bulk carbohydrate (mg g^{-1}), chlorophyll *a* (mg m^{-2}), fine fraction in surface sediment ($\% < 10\ \mu$m) and dry bulk density (kg m^{-3}).

CHAPTER 5

DISCUSSION

5.1 Size sorting by biofilms during erosion

Results from this study (figure 4.9) demonstrated that biofilms preferentially retained clays (< 4 μm) and cohesive silts (4-10 μm) (*sensu McCave et al.* (1995)) at low shear stresses (0.08 and 0.16 Pa), with associated changes to seabed texture. The intertidal mudflat under study, in fact, showed finer surface sediment when carbohydrate content, a measure of EPS levels and thus of biofilm abundance in the sediment, was greater (figure 4.12). EPS levels and the fine fraction of surface sediment were also found to be negatively correlated with dry bulk density (figure 4.12), suggesting that sediments are more porous when biofilms are more abundant. One possible explanation for this association is that biofilms increased porosity by filling space in the sediment with organic gels, however, finer sediments also naturally exhibit higher porosity than coarser sediments, making it impossible to distinguish the relative contributions of both physical and biological factors to porosity.

Observations from this study are in contrast with results from *Garwood et al.* (2013) who found biofilms to preferentially retain fine and medium silts (8 and 16 μm) at intermediate shear stresses (0.24, 0.32 and 0.40 Pa). This study was, however, conducted on a mudflat, while the latter study took place on a sandy flat. Taken together, these results may help refine a positive feedback outlined by *van de Koppel et al.* (2001). These authors described a positive feedback between silt content and diatom growth, where diatom mats increase the silt content of the sediment via increased silt flocculation and retention, which then supports higher microbial growth due to enhanced nutrient availability. This feedback would lead to either silt- or sand-dominated environments, both in a stable state until

sufficient silt is removed or supplied by physical factors. The results of the studies above, however, suggest that biofilms display different behaviour in silt-dominated and sand-dominated environments, which could further contribute to the positive feedback. Mud biofilms appear to retain finer particles than sand biofilms, with sorting taking place at lower shear stresses in the former. These characteristics seem particularly suited to maintain the substrate in a stable state, as the grain sizes retained in mud are cohesive, but those retained in fine sands are not (*van Ledden et al.*, 2004; *McCave and Hall*, 2006; *Law et al.*, 2008). *Garwood et al.* (2013) suggested that such a scenario could be caused by sand environments mainly hosting cyanobacteria that preferentially glue down coarser grains, and mud environments hosting diatoms that retain fine sediment, based on the dominant species reported by *Stal* (2010) for each environment. *Devitt* (2012), however, showed that a diatom monoculture of *Navicula pelliculosa* grown on sands also preferentially retained silts rather than clays. There may, therefore, be an association between sediment texture and biofilm pore sizes, which *Arnon et al.* (2010) hypothesized could determine the grain sizes preferentially retained by the biological matrix. Nevertheless, further research on the interactions between seabed texture and biofilm behaviour is necessary to develop a mechanistic description of biofilm effects on sediment sorting.

5.2 Seasonal mudflat erodibility

Overall, the higher mass of sediment resuspended from treated cores than from the corresponding untreated cores is consistent with previous studies that reported biofilms to increase sediment stability, both in the lab and in the field (*Holland et al.*, 1974; *Grant et al.*, 1986; *Sutherland et al.*, 1998b; *Lundkvist et al.*, 2007; *Garwood et al.*, 2013). The fact that the mass eroded from treated cores did not vary significantly over the study period also indicate that the change in the erodibility of untreated cores can be attributed to biological factors.

The high natural sediment erosion rates observed on June 24 (figure 4.1) show that biological factors other than biofilms, including *Corophium*, can contribute to sediment erosion. *Daborn et al.* (1993) conducted a study at Starrs Point, a nearby intertidal flat in the Minas Basin, and reported reduced erosion rates with declining *Corophium* numbers. The authors explained their results with a trophic cascade, where the arrival of semi-palmated sandpipers reduced *Corophium* abundance and, thus, grazing of biofilms. The

subsequent recovery of biofilms, they argued, was likely the cause of the reduced erosion observed, as biofilms are known to increase sediment stability. Results from this study, however, suggest an alternate mechanism. If the increased sediment erosion observed on June 24 had been caused by biofilm grazing, the treated cores should have displayed erosion levels much closer to those of the untreated cores. Moreover, the chlorophyll *a* and bulk carbohydrate data do not support a drastic reduction in biofilm levels. *Hamilton et al.* (2006) also reported a top-down control of sandpipers on *Corophium* with no effect on diatom biomass, and showed that the interactions between sandpipers, *Corophium* and biofilms did not translate into a trophic cascade in the Minas Basin. *Corophium* behaviour is thus more likely to have caused sediment resuspension on June 24 than reduced biofilm levels. In treated cores, this behaviour would have been inhibited by bleach, which killed all organisms, including *Corophium*. *Miller et al.* (1992) described changes in the feeding behaviour of macrofauna initiated by flow variations. It is thus possible that filling the cores prior to erosion, or the flow induced by the Gust microcosm, triggered feeding behaviour in *Corophium*, resulting in sediment resuspension or loosening of the sediment matrix. Further studies are required to fully understand the role of *Corophium* behaviour on sediment resuspension in the Bay of Fundy.

Attributing the high erosion observed on September 5 to rainfall is consistent with other studies that have shown rain to reduce critical erosion stresses of biofilm-covered sediment *in situ* (*Paterson et al.*, 1990, 2000; *Tolhurst et al.*, 2008b) and enhance erosion both in intertidal mudflats (*Pilditch et al.*, 2008) and salt marshes (*Mwamba and Torres*, 2002). The overall seasonal trend, excluding June 24 and September 5 (already discussed), shows that flat erodibility decreased from April to November 2012 (figure 4.5). This trend did not correlate with chlorophyll *a* and carbohydrate concentrations in the sediment, which is in contrast with previous studies (*Sutherland et al.*, 1998a,b; *Tolhurst et al.*, 2008a). The range of bulk carbohydrate concentrations observed in this study, however, varied approximately by a factor of 2, while other bulk carbohydrate measurements varied by a factor as high as 10 (*Sutherland et al.*, 1998b). The range of variation was, nevertheless, close to ranges reported for colloidal carbohydrate measurements, which varied by factors of 3-4 (*Sutherland et al.*, 1998a; *Tolhurst et al.*, 2008a). The difference in results might, therefore, be linked to the fact that laboratory studies use sediment of constant grain sizes when measuring the effect of biofilm on erodibility, while this study found biofilms to

modify the grain size of the seabed. Further research is required to address the implications of this interaction.

Nonetheless, the lack of correlation between carbohydrate levels and TME suggests that biofilms are not the only biological mechanism reducing flat erodibility. At the onset of the study, erodibility was high and bulk carbohydrate concentrations in the mid-range (figure 4.5 and 4.10). The high erodibility could be explained by fresh deposition of loose sediment, following ice melting, spring freshets (*Amos*, 1987), and a decrease in wind-generated waves from winter to summer (*Mulligan et al.*, submitted). In early spring, such sediment would not have been heavily subjected to the stabilization effects of biological processes. Then, biofilm growth may have initiated the stabilization process, but other biological processes are required to account for the decrease in erodibility as EPS levels began to decline.

The peak in bulk carbohydrate on June 9 is quickly followed by a peak in *Corophium* abundance (figure 4.10 and 4.4). Pelletization of the sediment by grazers and other macrofauna could, therefore, account for the decrease in erodibility observed from April to September (figure 4.5), as the sediment matrix is gradually processed into dense pellets with higher settling velocities than flocs. Although some studies reported pelletization by macrofauna enhancing sediment erodibility (*Andersen*, 2001; *Andersen et al.*, 2005), work in the York River estuary by *Friedrichs et al.* (2008) support the hypothesis that pelletization can reduce sediment erodibility. The further reduction in erodibility, observed from September to November, coincided with an increase in bulk carbohydrate, indicating that biofilm growth further increased sediment stability. At this point, high erosional stresses from waves associated with winter storms (*Amos*, 1987; *Mulligan et al.*, submitted), as well as scouring by sediment-laden ice blocks were likely required for the sediment matrix to be broken down and resuspended.

Tao (2013) reported highest sediment concentrations in the Minas Basin in March, and lowest concentrations in late summer, early fall. The results of this study suggest that reduced flat erodibility could account for the decrease in sediment concentration from March to August, but an additional mechanism must be invoked to account for the increase in sediment concentrations in the fall, when flat erodibility is low. *Amos* (1987) stated cliff and seabed erosion as the two main sources of suspended sediment in Chignecto Bay, Bay of Fundy. It is, therefore, reasonable to assume that similar processes govern suspended

sediment in the Minas Basin. *Mulligan et al.* (submitted) reported higher wind-driven waves in winter than in summer, which implies higher bed shear stresses, and thus greater erosion, in the winter than in the summer. This could result in higher sediment resuspension in the winter, despite the lower mudflat erodibility observed. The results of this study imply that biological processes dictate flat erodibility in the Bay of Fundy, but put in context of other studies (*Tao*, 2013; *Mulligan et al.*, submitted), it must be concluded that the influence of these biological processes on large-scale suspended sediment concentrations are mainly governed by physical factors. Combining the observations of this study with a model of bed shear stress in the area would shed more light on this issue.

CHAPTER 6

CONCLUSIONS

Mudflat biofilms reduced erosion and preferentially retained clays (< 4 μm) and cohesive silts (4-10 μm) when subjected to low erosion shear stresses (0.08 and 0.16 Pa), resulting in a fining of surface sediment at the site when thick biofilms were present. This is in contrast with sand biofilms that were previously reported to preferentially retain fine and medium silts (*Garwood et al.*, 2013), suggesting that microbial mats help maintain their substrate in a stable state. Results from June 24 indicated that *Corophium*, a keystone species in the Bay of Fundy, could induce sediment resuspension by means other than biofilm grazing. Limited data, however, warrants further investigation. Finally, an overall decrease in flat erodibility from April to November 2012 was reported. As this trend was not correlated with sediment carbohydrate and chlorophyll quotas, pelletization by grazers and macrofauna was invoked as a mechanism for reducing flat erodibility from April to September because biological processes were shown to be sufficient to explain the variation in mudflat erodibility throughout the study period. The decrease in flat erodibility observed from September to November, however, was attributed to biofilm growth.

Further research is necessary to fully evaluate the effects of *Corophium* and pelletization on mudflat erodibility in the Bay of Fundy, as *Corophium* abundance was overall low at this site and pellets were not quantified during this study. The overall effect of biological processes on seasonal suspended sediment concentrations in the Minas Basin will also be better assessed when erodibility measurements from this study are combined with models of bed shear stresses in the area.

APPENDIX A

DATA FOR ALL CORES

This appendix includes all grain size data collected for every field day. Data from both untreated and treated cores are included. DIGS distributions of the eroded sediment are plotted in terms of cumulative concentrations (cumulative PPM), which means that each curve represents the total concentration of sediment resuspended by shear stresses $\leq$ to the stress by which it is labelled.

No surface data available for April 27, 2012.

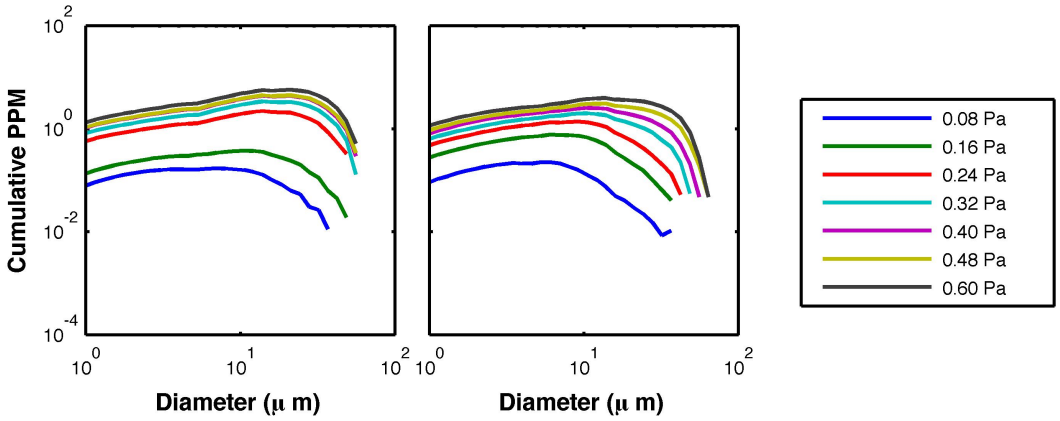

No mobility distributions available for April 27, 2012.

Figure A.1: Grain size data collected on April 27, 2012. Because no surface sediment was collected, only cumulative concentrations (in ppm) are available for that date.

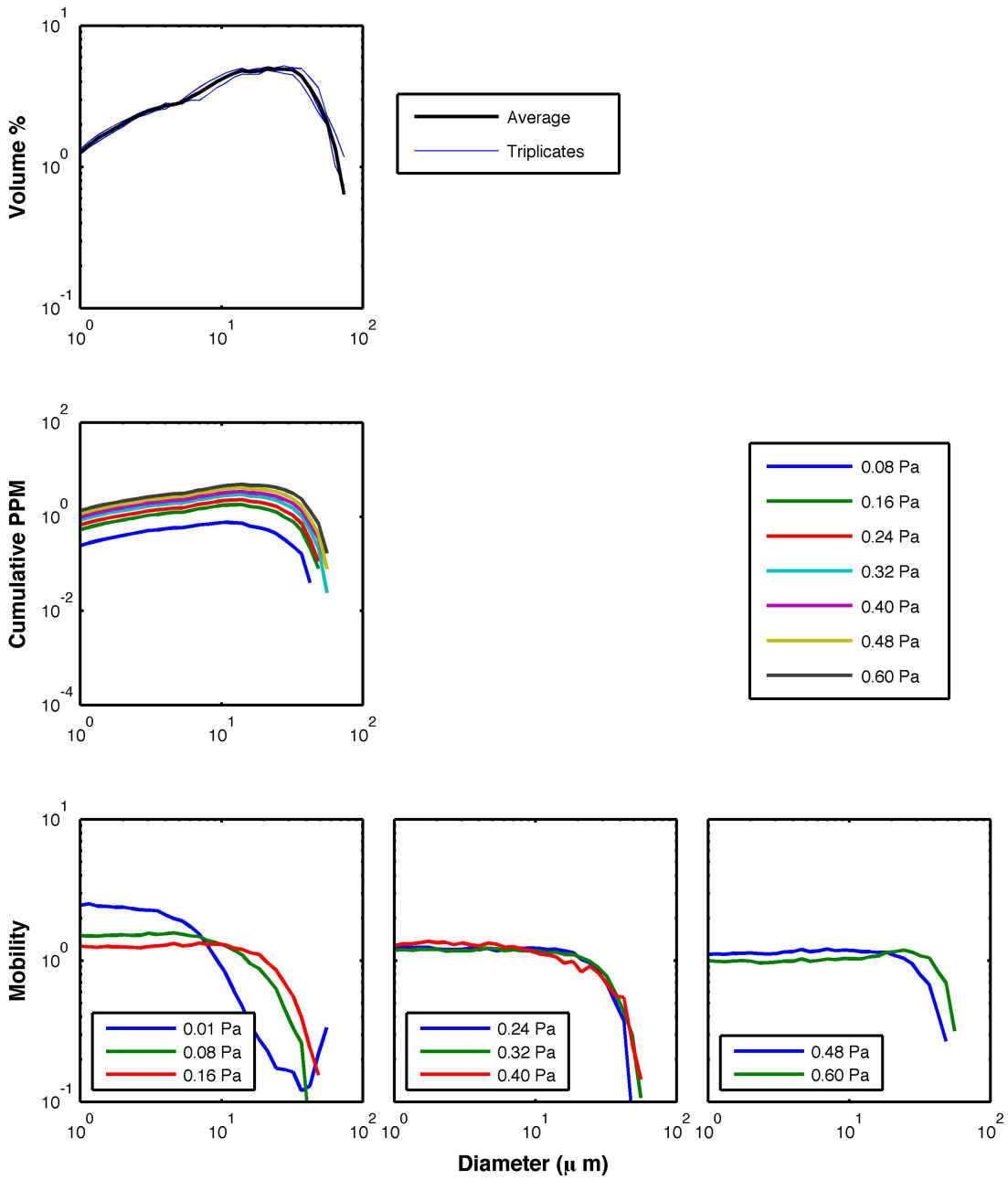

Figure A.2: Grain size data collected on May 11, 2012. The top row shows surface DIGS, the second row cumulative concentrations (in ppm), and the third row shows grain size mobilities.

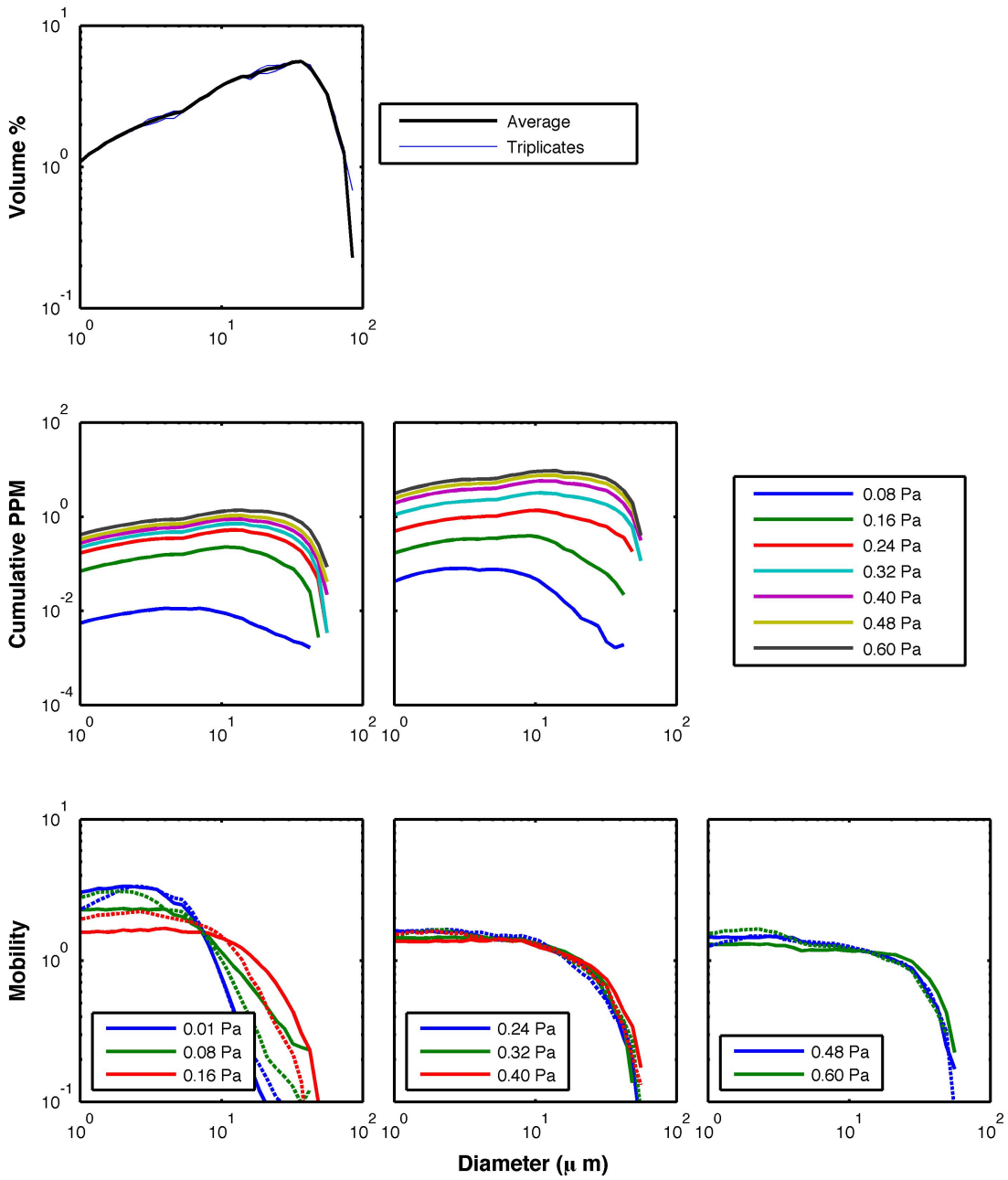

Figure A.3: Grain size data collected on May 26, 2012. The top row shows surface DIGS, the second row cumulative concentrations (in ppm), and the third row shows grain size mobilities. The left panel on the second row shows data for untreated cores and the right panel for treated cores, while the solid lines in the third row represent untreated cores and the dashed lines treated cores.

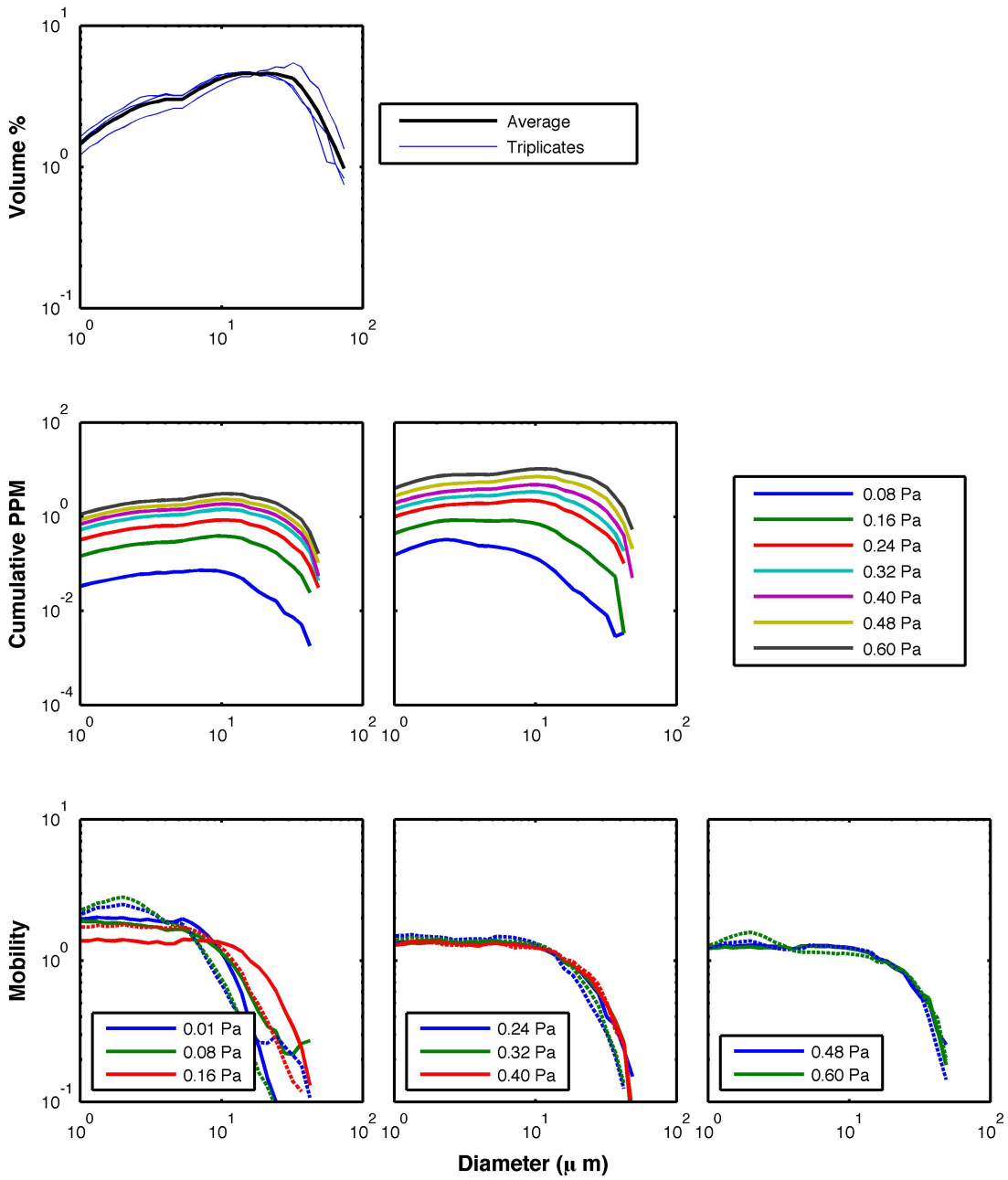

Figure A.4: Grain size data collected on June 9, 2012. The top row shows surface DIGS, the second row cumulative concentrations (in ppm), and the third row shows grain size mobilities. The left panel on the second row shows data for untreated cores and the right panel for treated cores, while the solid lines in the third row represent untreated cores and the dashed lines treated cores.

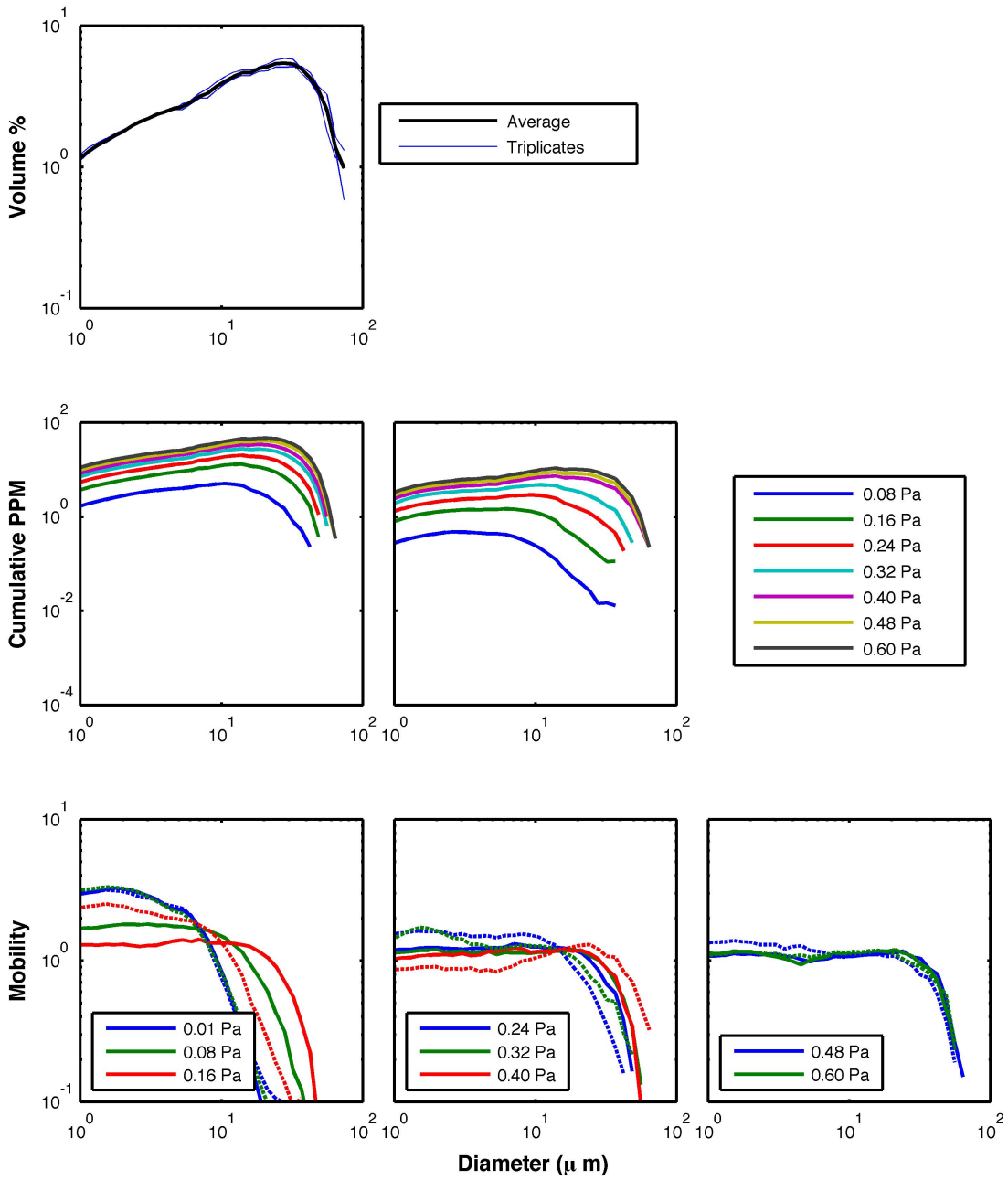

Figure A.5: Grain size data collected on June 24, 2012. The top row shows surface DIGS, the second row cumulative concentrations (in ppm), and the third row shows grain size mobilities. The left panel on the second row shows data for untreated cores and the right panel for treated cores, while the solid lines in the third row represent untreated cores and the dashed lines treated cores.

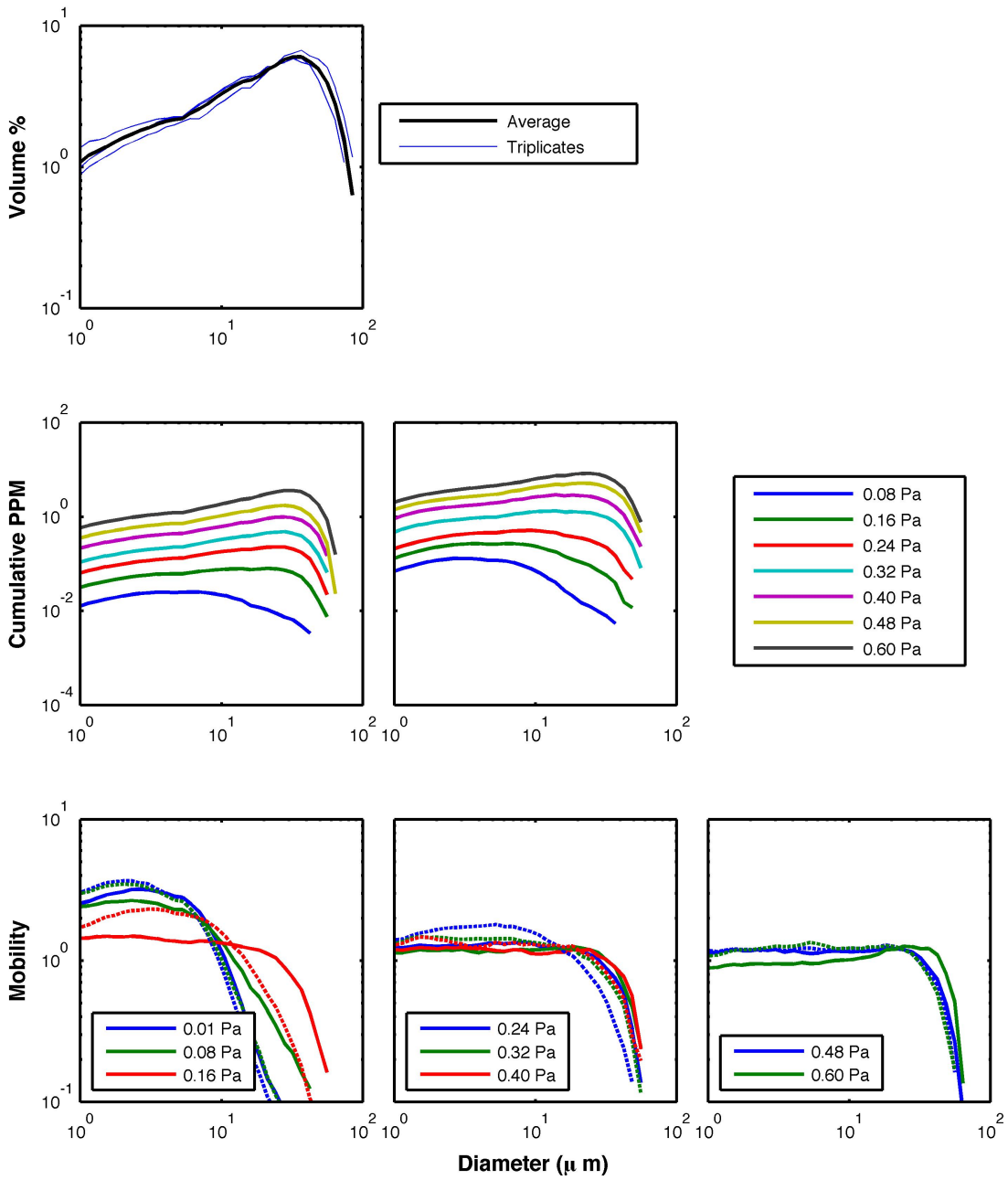

Figure A.6: Grain size data collected on July 9, 2012. The top row shows surface DIGS, the second row cumulative concentrations (in ppm), and the third row shows grain size mobilities. The left panel on the second row shows data for untreated cores and the right panel for treated cores, while the solid lines in the third row represent untreated cores and the dashed lines treated cores.

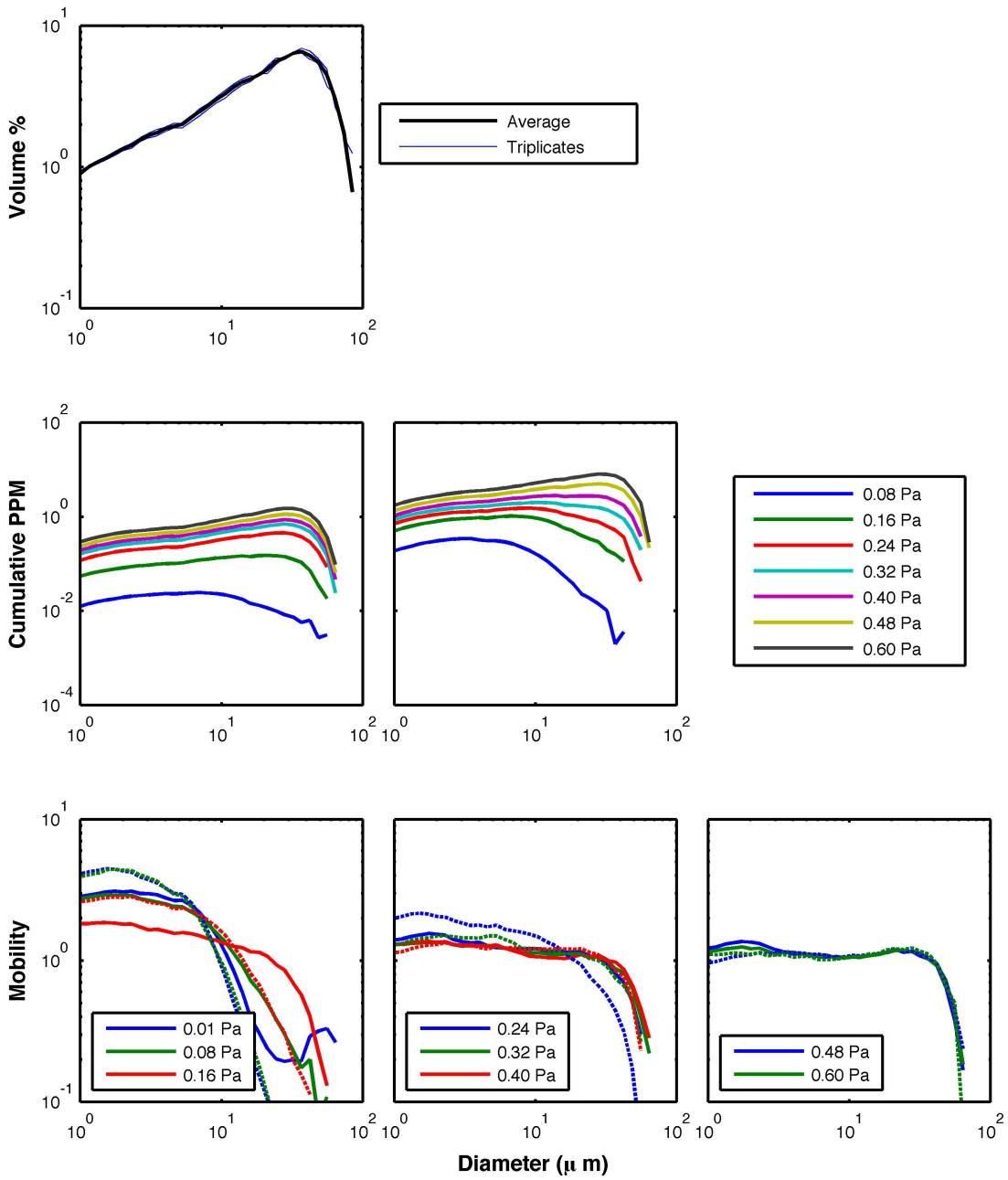

Figure A.7: Grain size data collected on July 24, 2012. The top row shows surface DIGS, the second row cumulative concentrations (in ppm), and the third row shows grain size mobilities. The left panel on the second row shows data for untreated cores and the right panel for treated cores, while the solid lines in the third row represent untreated cores and the dashed lines treated cores.

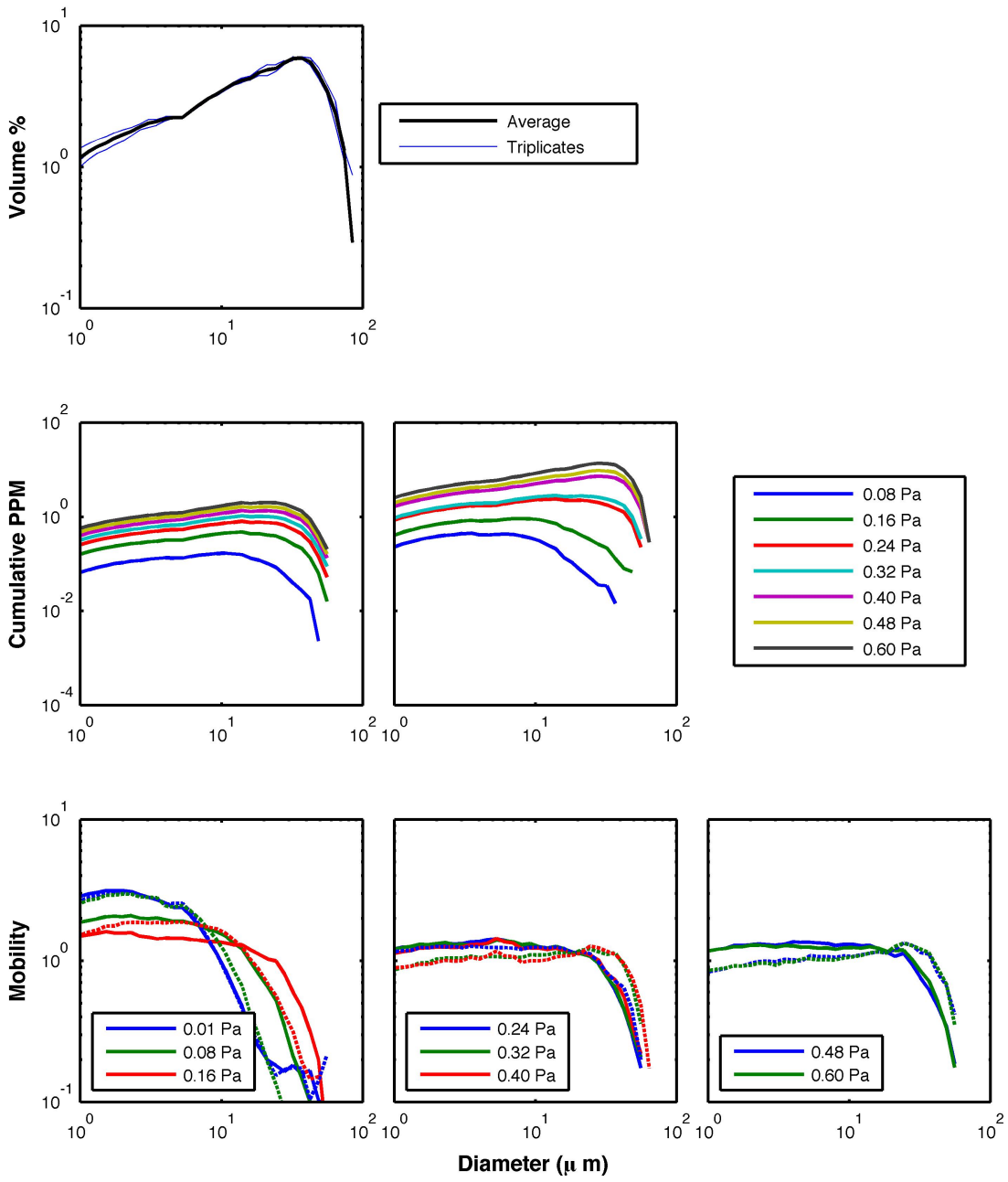

Figure A.8: Grain size data collected on August 8, 2012. The top row shows surface DIGS, the second row cumulative concentrations (in ppm), and the third row shows grain size mobilities. The left panel on the second row shows data for untreated cores and the right panel for treated cores, while the solid lines in the third row represent untreated cores and the dashed lines treated cores.

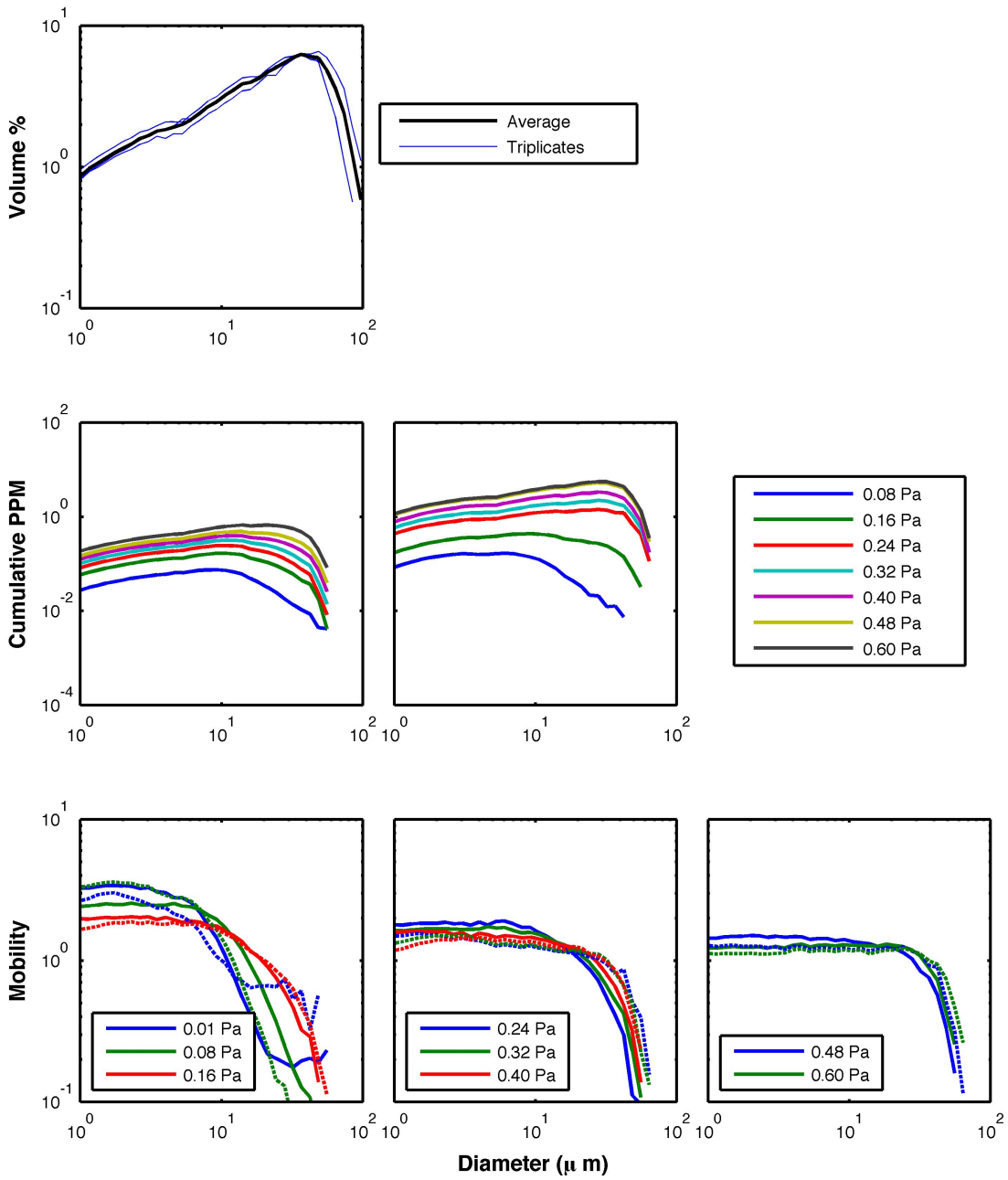

Figure A.9: Grain size data collected on August 22, 2012. The top row shows surface DIGS, the second row cumulative concentrations (in ppm), and the third row shows grain size mobilities. The left panel on the second row shows data for untreated cores and the right panel for treated cores, while the solid lines in the third row represent untreated cores and the dashed lines treated cores.

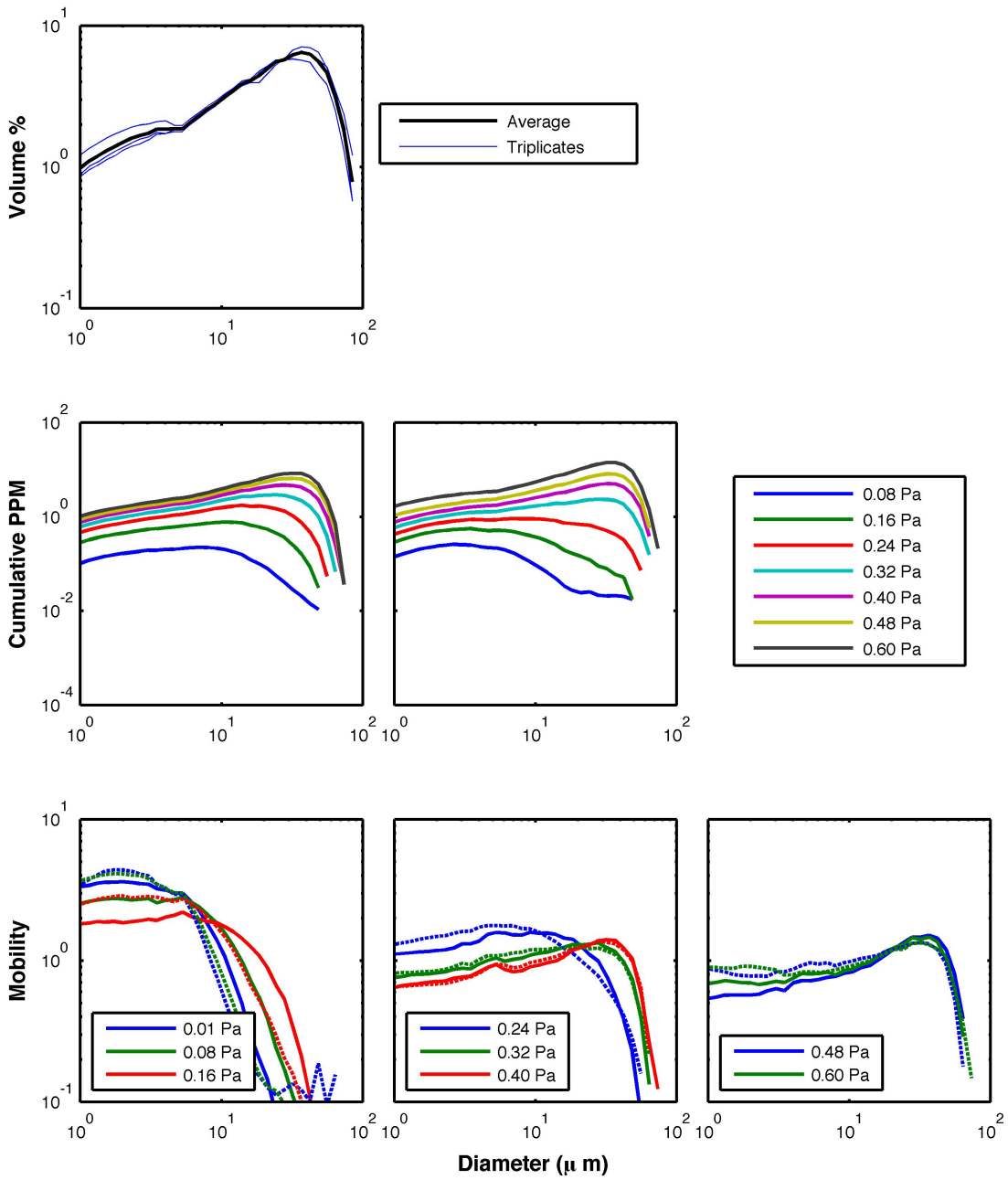

Figure A.10: Grain size data collected on September 5, 2012. The top row shows surface DIGS, the second row cumulative concentrations (in ppm), and the third row shows grain size mobilities. The left panel on the second row shows data for untreated cores and the right panel for treated cores, while the solid lines in the third row represent untreated cores and the dashed lines treated cores.

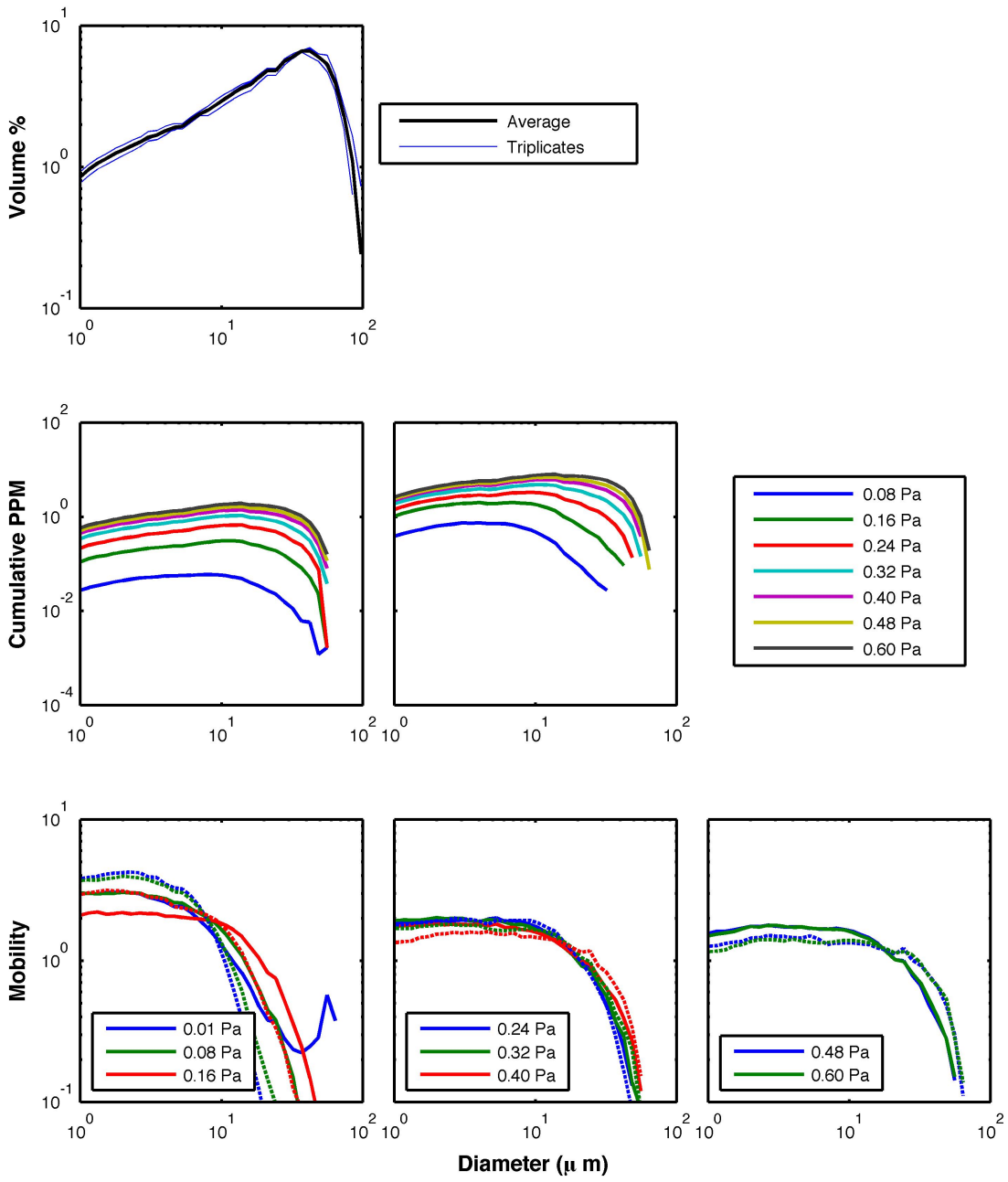

Figure A.11: Grain size data collected on September 22, 2012. The top row shows surface DIGS, the second row cumulative concentrations (in ppm), and the third row shows grain size mobilities. The left panel on the second row shows data for untreated cores and the right panel for treated cores, while the solid lines in the third row represent untreated cores and the dashed lines treated cores.

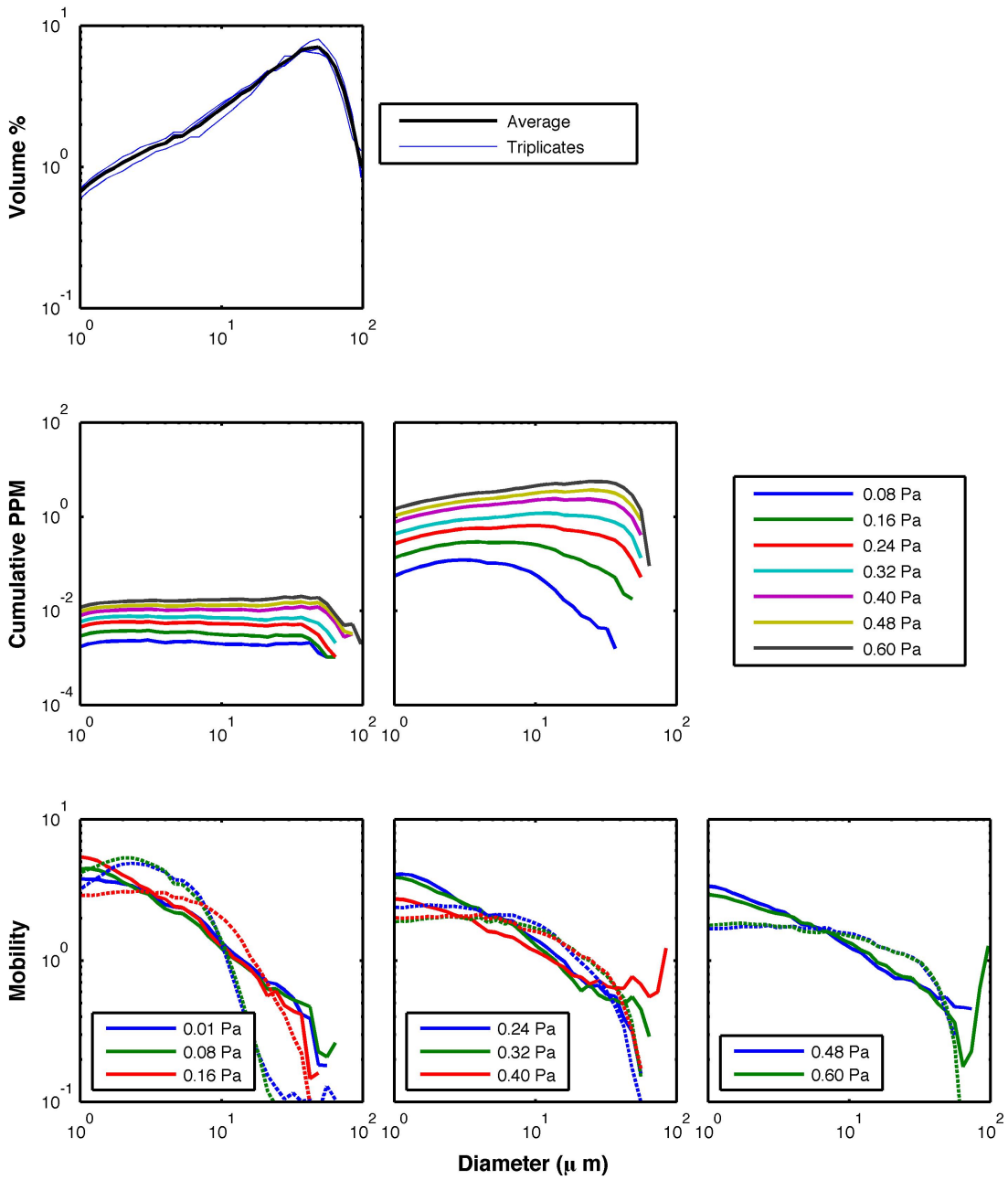

Figure A.12: Grain size data collected on October 6, 2012. The top row shows surface DIGS, the second row cumulative concentrations (in ppm), and the third row shows grain size mobilities. The left panel on the second row shows data for untreated cores and the right panel for treated cores, while the solid lines in the third row represent untreated cores and the dashed lines treated cores.

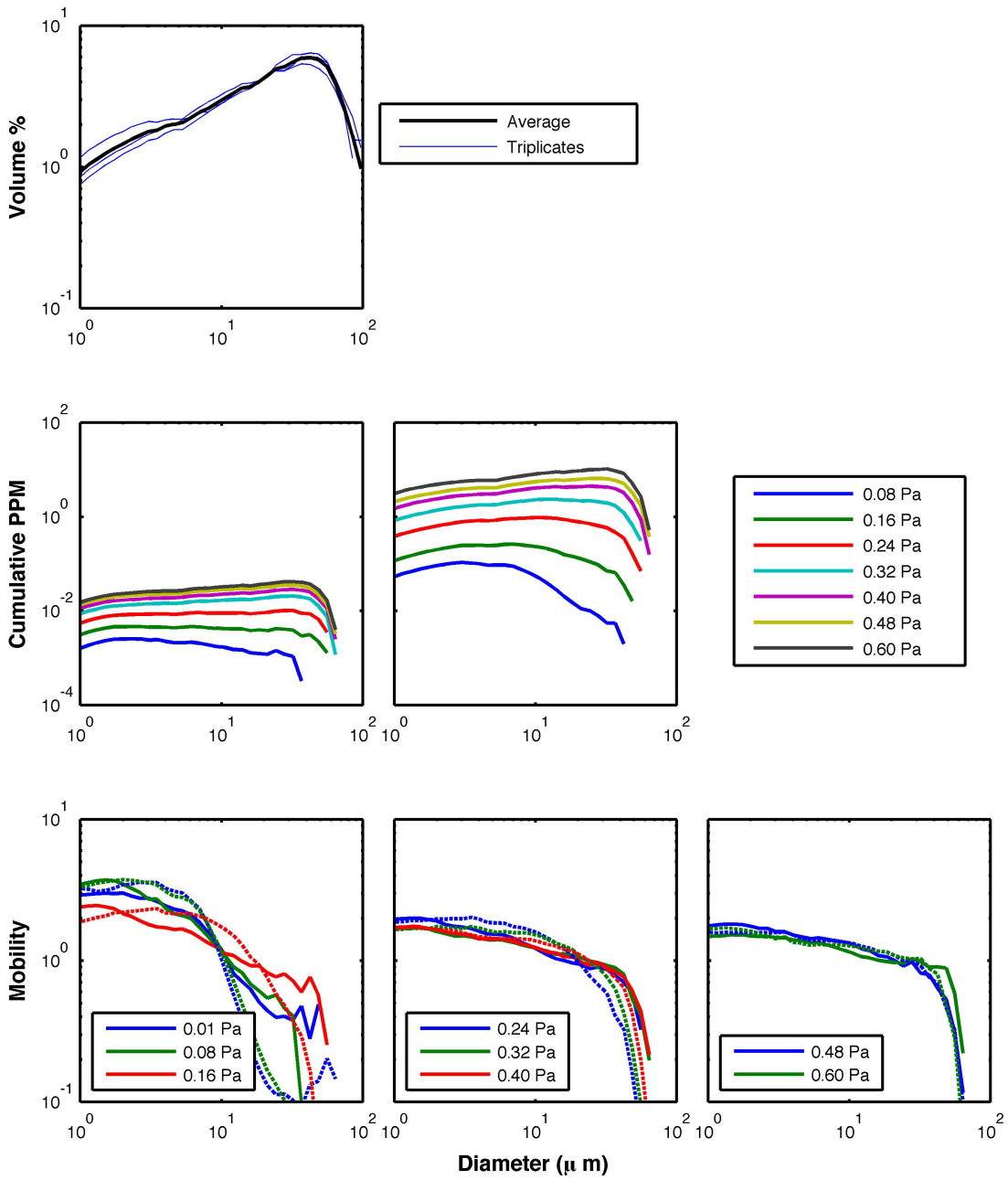

Figure A.13: Grain size data collected on October 20, 2012. The top row shows surface DIGS, the second row cumulative concentrations (in ppm), and the third row shows grain size mobilities. The left panel on the second row shows data for untreated cores and the right panel for treated cores, while the solid lines in the third row represent untreated cores and the dashed lines treated cores.

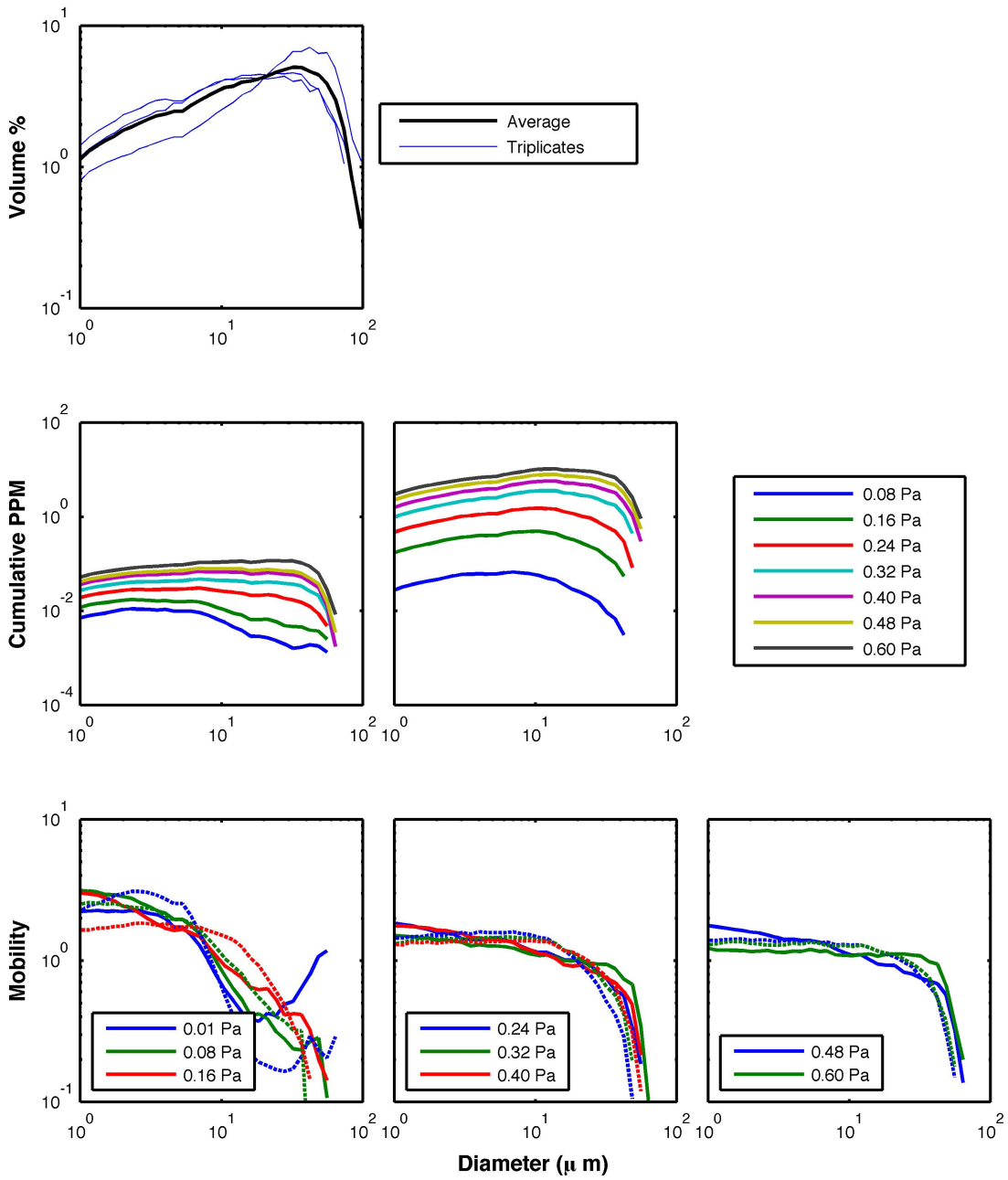

Figure A.14: Grain size data collected on November 6, 2012. The top row shows surface DIGS, the second row cumulative concentrations (in ppm), and the third row shows grain size mobilities. The left panel on the second row shows data for untreated cores and the right panel for treated cores, while the solid lines in the third row represent untreated cores and the dashed lines treated cores.

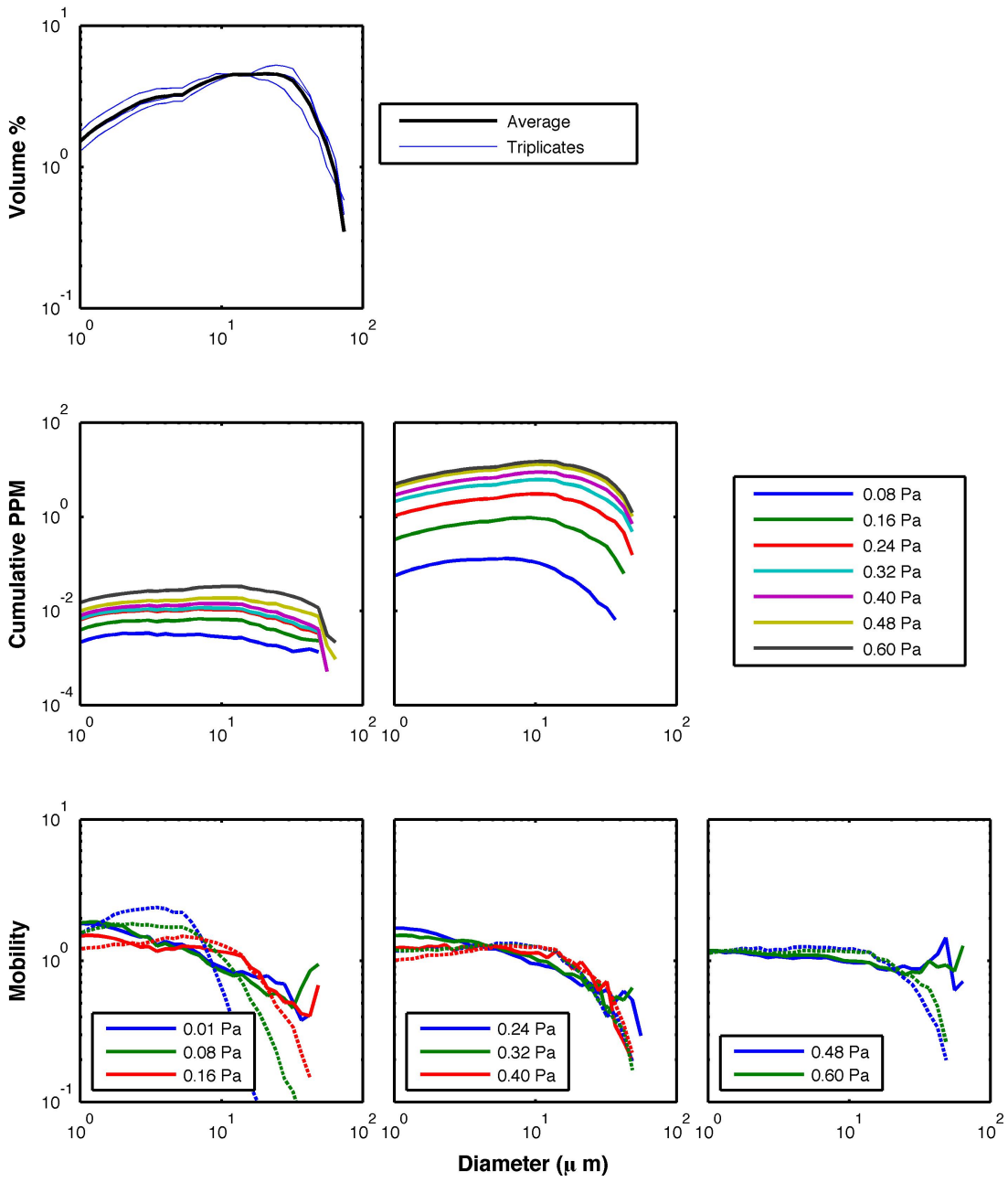

Figure A.15: Grain size data collected on November 20, 2012. The top row shows surface DIGS, the second row cumulative concentrations (in ppm), and the third row shows grain size mobilities. The left panel on the second row shows data for untreated cores and the right panel for treated cores, while the solid lines in the third row represent untreated cores and the dashed lines treated cores.

APPENDIX B

ADVICE FOR PHENOL-SULPHURIC ASSAY

As part of this thesis work, a significant amount of time was spent trying to obtain good standard curves for the phenol-sulphuric assay. Advice from Dr. Hugh MacIntyre, Dr. Jon Grant, Cathy Ryan, Trina Whitsitt, and results from experimental learning were pooled to produce this informal guide to obtaining good standard curves. Including it in this thesis was meant to save time to someone wanting to repeat the procedure.

Lessons learned from my carbohydrate experience

An unofficial guide to obtaining good standard curves

Avoid plastic wherever possible:

- Use test tubes made of glass.
- Weigh the solid phenol in a 20 ml glass beaker.
- Only use Eppendorf centrifuge tubes for the centrifugation.
- Use glass or quartz cuvettes for the spectrophotometer (a set can be found in the carbohydrate cupboard with better lids than the one I used).

Phenol:

- Keep the solid phenol in the fridge. Do not allow it to warm up to room temperature.
- Weigh the solid phenol into a 20 ml glass beaker, add water to the beaker before transferring to a volumetric flask, or add water using a pipette.
- Bear in mind that 0.5 ml of phenol is required per sample and standard curve tube avoid making too much phenol this way.
- Using a metal spatula to weigh the phenol is fine.
- Keep the freshly made phenol in an amber bottle (mouth wide enough for 25 ml repeater pipette tip).

Doubling the reagents:

- Doubling the reagents in a 10-ml test tube is fine.
- Vortex for 20 seconds per sample (instead of 5-10 s) when doing so.

Smooth flow to the day:

- I always started with making my phenol solution rather than my glucose solution, to avoid contamination. (Cheaper to remake glucose than phenol if I forgot to rinse the spatula thoroughly.)
- To generate my phenol, I liked to weigh 1.25 g of phenol for each 25 ml of water I would add, using the 25 ml glass pipette and a pipette bulb.

- To generate my glucose stock, I liked to dissolve 1 g of glucose in a 500 ml flask with DI water, then pipette 20 ml of this solution into a 200 ml flask, using the 20 ml glass pipette and a pipette bulb.
- Use a new 25 ml repeater pipette tip for the phenol.
- Use a single new 10 ml repeater pipette tip for the DI water and glucose solution. Start with the DI water in all standards and samples, then glucose (rinse tip with glucose solution three times).
- Use 2 ml centrifuge tubes, this way there is enough supernatant that the glass cuvettes can be rinsed with a bit of the sample before pouring it in. Do not use water to rinse the cuvettes, as the supernatant is not very miscible in water.
- Tip the cuvettes up and down multiple times on the way to the spectrophotometer to ensure the sample is well mixed.
- Use a kimwipe to ensure the outside of the cuvette is clean before reading.

Good luck!

APPENDIX C

SORTABILITY INDEX

The sortability index presented in this thesis was developed during my Honours' research project. The full equations were already published in *Garwood et al.* (2013), but they are included in this appendix to provide the reader with all the information necessary to fully understand the work presented in this thesis. As mentioned in section 3.2, the index describes mobility distributions, where mobility is plotted as a function of grain diameter (μm). The index can be thought of as the slope of this relationship, because large positive values indicate coarser grains being preferentially resuspended, while large negative values indicate preferential resuspension of finer grains. Unlike a slope, however, the index will be different for two relatively flat mobility distributions when one distribution contains larger grains than the other and will also describe distributions with peaks.

To calculate the sortability index, the total sum of squares was first obtained for a given distribution:

$$|S_I| = \sum_{i=1}^{nclass} (M_{i,\tau} - \bar{M}_\tau)^2, \tag{C.1}$$

where i represents a given size class, τ is the stress applied by the Gust microcosm, and $\bar{M}_\tau$ represents the average mobility at a given stress. The sign of the index was then determined by comparing the total variation of the data points above and below the midpoint, within a single mobility distribution.

$$
\begin{aligned}
v_b &= \sum_{i=1}^{m-1} (M_{i,\tau} - \bar{M}_\tau) \\
v_a &= \sum_{i=m+1}^{nclass} (M_{i,\tau} - \bar{M}_\tau)
\end{aligned}
\tag{C.2}
$$

where v_b is the variation below the midpoint, v_a is the variation above the midpoint, and m is the midpoint (i.e. mid-size class). Equations C.2 differ from equation C.1 in that the terms are not squared and that only half of the distribution is considered at a time. This is to identify toward which end of the distribution mobilities dip (negative variation) or rise (positive variation). If $v_b < v_a$, then the distribution shows higher mobility values at grain sizes larger than the midpoint, implying that coarser grains were preferentially resuspended. The previously calculated S_I was assigned a positive value. Alternately, if $v_b > v_a$, then the distribution shows higher mobility values at grain sizes smaller than the midpoint, implying that finer grains were preferentially resuspended, and S_I was assigned a negative value.

BIBLIOGRAPHY

Amos, C. L., Fine-grained sediment transport in chignecto bay, bay of fundy, canada, *Continental Shelf Research*, *7*, 1295–1300, 1987.

Andersen, T., Seasonal variation in erodibility of two temperate, microtidal mudflats, *Estuarine Coastal and Shelf Science*, *53*, 1–12, 2001.

Andersen, T. J., L. C. Lund-Hansen, M. Pejrup, K. T. Jensen, and K. N. Mouritsen, Biologically induced differences in erodibility and aggregation of subtidal and intertidal sediments: a possible cause for seasonal changes in sediment deposition, *Journal of Marine Systems*, *55*, 123–138, 2005.

Arnon, S., L. P. Marx, K. E. Searcy, and A. I. Packman, Effects of overlying velocity, particle size, and biofilm growth on stream-subsurface exchange of particles, *Hydrological Processes*, *24*, 108–114, 2010.

Baker, E. T., and J. W. Lavelle, The effect of particle-size on the light attenuation coefficient of natural suspensions, *Journal of Geophysical Research-Oceans*, *89*, 8197–8203, 1984.

Bender, J., S. Rodriguezeaton, U. M. Ekanemesang, and P. Phillips, Characterization of metal-binding bioflocculants produced by the cyanobacterial component of mixed microbial mats, *Applied and Environmental Microbiology*, *60*, 2311–2315, 1994.

Boss, E., M. Twardowski, and S. Herring, Shape of the particulate beam attenuation spectrum and its inversion to obtain the shape of the particulate size distribution, *Applied Optics*, *40*, 4885–4893, 2001.

da S. Quaresma, V., C. L. Amos, and M. Flindt, The influences of biological activity and consolidation time on laboratory cohesive beds, *Journal of Sedimentary Research*, *74*, 184–190, 2004.

Daborn, G. R., et al., An ecological cascade effect - Migratory birds affect stability of intertidal sediments, *Limnology and Oceanography*, *38*, 225–231, 1993.

Decho, A. W., Microbial biofilms in intertidal systems: an overview, *Continental Shelf Research*, *20*, 1257–1273, 2000.

Devitt, K., Do diatom biofilms retain fine-grained sediment?, Honours Thesis, Dalhousie University, 2012.

Dubois, M., K. A. Gilles, J. K. Hamilton, P. A. Rebers, and F. Smith, Colorimetric method for determination of sugars and related substances, *Analytical Chemistry*, *28*, 350–356, 1956.

Elner, R., P. Beninger, D. Jackson, and T. Potter, Evidence of a new feeding mode in western sandpiper (*Calidris mauri*) and dunlin (*Calidris alpina*) based on bill and tongue morphology and ultrastructure, *Marine Biology*, *146*, 1223–1234, 2005.

Faas, R., H. Christian, G. R. Daborn, and M. Brylinsky, *Biological-control of mass properties of surficial sediments: An example from Starr's Point tidal flat, Minas Basin, Bay of Fundy*, pp. 360–377, In: A.J. Mehta (Ed.), Nearshore and Estuarine Cohesive Sediment Transport, American Geophysical Union, Washington, D. C., 1993.

Folk, R. L., The distinction between grain size and mineral composition in sedimentary-rock nomenclature, *Journal of Geology*, *62*, 344–359, 1954.

Friedrichs, C. T., G. M. Cartwright, and P. J. Dickhudt, Quantifying benthic exchange of fine sediment via continuous, noninvasive measurements of settling velocity and bed erodibility, *Oceanography*, *21*, 168–172, 2008.

Garwood, J. C., P. S. Hill, and B. A. Law, Biofilms and size sorting of fine sediment during erosion in intertidal sands, *Estuaries and Coasts*, *36*, 1024–1036, 2013.

Goericke, R., and D. Repeta, Chlorophyll-a and chlorophyll-b and divinyl chlorophyll-a and chlorophyll-b in the open subtropical north-atlantic ocean, *Marine Ecology Progress Series*, *101*, 307–313, 1993.

Grant, J., U. V. Bathmann, and E. L. Mills, The interaction between benthic diatom films and sediment transport, *Estuarine Coastal and Shelf Science*, *23*, 225–238, 1986.

Greenberg, D. A., and C. L. Amos, Suspended sediment transport and deposition modeling in the Bay of Fundy, Nova Scotia - a region of potential tidal power development, *Canadian Journal of Fisheries and Aquatic Sciences*, *40*, 20–34, 1983.

Guo, Z., X. Hua, X. Lan, Y. Sun, and D. Dong, Evidence for a mutual effect of biofilms, suspended particles and sediments on DDT sorption, *Environmental Chemistry Letters*, *10*, 407–411, 2012.

Hamilton, D. J., A. W. Diamond, and P. G. Wells, Shorebirds, snails, and the amphipod (*Corophium volutator*) in the upper Bay of Fundy: top-down vs. bottom-up factors, and the influence of compensatory interactions on mudflat ecology, *Hydrobiologia*, *567*, 285–306, 2006.

Hicklin, P. W., D. L. Peer, L. E. Linkletter, and Marine Ecology Laboratory, *Distribution and abundance of* Corophium volutator *(Pallas),* Macoma balthica *(L.) and* Heteromastus filiformis *(Clarapede) in the intertidal zone of Cumberland Basin and Shepody Bay, Bay of Fundy*, Canadian technical report of fisheries and aquatic sciences, ISSN:0706-6457, no. 965, Public Archives, Canada, Ottawa, 1980.

Holland, A. F., R. G. Zingmark, and J. M. Dean, Quantitative evidence concerning stabilization of sediments by marine benthic diatoms, *Marine Biology*, *27*, 191–196, 1974.

Hooker, S., et al., The Fifth SeaWiFS HPLC Analysis Round-Robin Experiment (SeaHARRE-5), *Nasa tech. memo 2012-217503*, NASA Goddard Space Flight Center, Greenbelt, Maryland, 2012.

Langdon, C., On the causes of interspecific differences in the growth irradiance relationship for phytoplankton. ii. a general review, *Journal of Plankton Research*, *10*, 1291–1312, 1988.

Law, B. A., P. S. Hill, T. G. Milligan, K. J. Curran, P. L. Wiberg, and R. A. Wheatcroft, Size sorting of fine-grained sediments during erosion: Results from the western Gulf of Lions, *Continental Shelf Research*, *28*, 1935–1946, 2008.

Lundkvist, M., M. Grue, P. L. Friend, and M. R. Flindt, The relative contributions of physical and microbiological factors to cohesive sediment stability, *Continental Shelf Research*, *27*, 1143–1152, 2007.

McCave, I. N., and I. R. Hall, Size sorting in marine muds: Processes, pitfalls, and prospects for paleoflow-speed proxies, *Geochemistry Geophysics Geosystems*, *7*, Q10N05, 2006.

McCave, I. N., B. Manighetti, and S. G. Robinson, Sortable silt and fine sediment size composition slicing - Parameters for paleocurrent speed and paleoceanography, *Paleoceanography*, *10*, 593–610, 1995.

Miller, D. C., M. J. Bock, and E. J. Turner, Deposit and suspension feeding in oscillatory flows and sediment fluxes, *Journal of Marine Research*, *50*, 489–520, 1992.

Milligan, T., and K. Kranck, *Electroresistance particle size analyzers*, pp. 109–118, In: J. Syvitski (Ed.), Principles, Methods, and Application of Particle Size Analysis, Cambridge University Press, Cambridge; New York, 1991.

Milligan, T., and D. Loring, The effect of flocculation on the size distributions of bottom sediment in coastal inlets: Implications for contaminant transport., *Water Air and Soil Pollution*, *99*, 33–42, 1997.

Mulligan, R., P. Smith, P. Hill, and J. Tao, Tidal current and wind-wave controls on suspended sediment concentrations in a macrotidal basin, *Journal of Geophysical Research*, submitted.

Mwamba, M. J., and R. Torres, Rainfall effects on marsh sediment redistribution, north inlet, south carolina, usa, *Marine Geology*, *189*, 267–287, 2002.

Paterson, D., et al., Variations in sediment properties, Skeffling mudflat, Humber Estuary, UK, *Continental Shelf Research*, *20*, 1373–1396, 2000.

Paterson, D. M., R. M. Crawford, and C. Little, Subaerial exposure and changes in the stability of intertidal estuarine sediments, *Estuarine Coastal and Shelf Science*, *30*, 541–556, 1990.

Piggot, A. M., J. S. Klaus, S. Johnson, M. C. Phillips, and H. M. Solo-Gabriele, Relationship between enterococcal levels and sediment biofilms at recreational beaches in South Florida, *Applied and Environmental Microbiology*, *78*, 5973–5982, 2012.

Pilditch, C. A., J. Widdows, N. J. Kuhn, N. D. Pope, and M. D. Brinsley, Effects of low tide rainfall on the erodibility of intertidal cohesive sediments, *Continental Shelf Research*, *28*, 1854–1865, 2008.

Shepherd, H. P. W. P. V. A., Philippa C., *Changes in sediment types and invertebrate fauna in the intertidal mudflats of the Bay of Fundy between 1977 and 1994*, Canadian Wildlife Service, Atlantic Region, Environmental Conservation Branch, Sackville, NB, 1995.

Slade, W. H., E. Boss, and C. Russo, Effects of particle aggregation and disaggregation on their inherent optical properties, *Optics Express*, *19*, 7945–7959, 2011.

Smith, D. J., and G. J. C. Underwood, Exopolymer production by intertidal epipelic diatoms, *Limnology and Oceanography*, *43*, 1578–1591, 1998.

Stal, L. J., Microphytobenthos as a biogeomorphological force in intertidal sediment stabilization, *Ecological Engineering*, *36*, 236–245, 2010.

Sun, M., Z. Qian, and W. Hu, On the method for determining total dissolved carbohydrates in sea water, temperature effect of phenol sulfuric acid method, *Collected Oceanic Works*, *7*, 1984.

Sutherland, I. W., *Biotechnology of Microbial Exopolysaccharides*, Cambridge University Press, Cambridge; New York, 1990.

Sutherland, T., C. Amos, and J. Grant, The effect of buoyant biofilms on the erodibility of sublittoral sediments of a temperate microtidal estuary, *Limnology and Oceanography*, *43*, 225–235, 1998a.

Sutherland, T. F., J. Grant, and C. L. Amos, The effect of carbohydrate production by the diatom *Nitzschia curvilineata* on the erodibility of sediment, *Limnology and Oceanography*, *43*, 65–72, 1998b.

Tao, J., Seasonal variability of total suspended matter in Minas Basin, Bay of Fundy, Master's thesis, Dalhousie University, 2013.

Thrush, S. F., and P. K. Dayton, Disturbance to marine benthic habitats by trawling and dredging: Implications for marine biodiversity, *Annual Review of Ecology and Systematics*, *33*, 449–473, 2002.

Tolhurst, T. J., K. S. Black, D. M. Paterson, H. J. Mitchener, G. R. Termaat, and S. A. Shayler, A comparison and measurement standardisation of four *in situ* devices for determining the erosion shear stress of intertidal sediments, *Continental Shelf Research*, *20*, 1397–1418, 2000.

Tolhurst, T. J., M. Consalvey, and D. M. Paterson, Changes in cohesive sediment properties associated with the growth of a diatom biofilm, *Hydrobiologia*, *596*, 225–239, 2008a.

Tolhurst, T. J., C. W. Watts, S. Vardy, J. E. Saunders, M. C. Consalvey, and D. M. Paterson, The effects of simulated rain on the erosion threshold and biogeochemical properties of intertidal sediments, *Continental Shelf Research*, *28*, 1217–1230, 2008b.

Trites, M., I. Kaczmarska, J. M. Ehrman, P. W. Hicklin, and J. Ollerhead, Diatoms from two macro-tidal mudflats in Chignecto Bay, Upper Bay of Fundy, New Brunswick, Canada, *Hydrobiologia*, *544*, 299–319, 2005.

Utne-Palm, A. C., Visual feeding of fish in a turbid environment: Physical and behavioural aspects, *Marine and Freshwater Behaviour and Physiology*, *35*, 111–128, 2002.

van de Koppel, J., P. M. J. Herman, P. Thoolen, and C. H. R. Heip, Do alternate stable states occur in natural ecosystems? Evidence from a tidal flat, *Ecology*, *82*, 3449, 2001.

van Ledden, M., W. G. M. van Kesteren, and J. C. Winterwerp, A conceptual framework for the erosion behaviour of sand-mud mixtures, *Continental Shelf Research*, *24*, 1–11, 2004.

Wiberg, P., D. Drake, and D. Cacchione, Sediment resuspension and bed armoring during high bottom stress events on the northern california inner continental-shelf - measurements and predictions, *Continental Shelf Research*, *14*, 1191–1219, 1994.

Wright, S. W., S. W. Jeffrey, R. F. C. Mantoura, C. A. Llewellyn, T. Bjornland, D. Repeta, and N. Welschmeyer, Improved HPLC method for the analysis of chlorophylls and carotenoids from marine-phytoplankton, *Marine Ecology Progress Series*, *77*, 183–196, 1991.

Wu, Y., J. Chaffey, D. A. Greenberg, K. Colbo, and P. C. Smith, Tidally-induced sediment transport patterns in the upper Bay of Fundy: A numerical study, *Continental Shelf Research*, *31*, 2041–2053, 2011.